Available online at www.sciencedirect.com
ScienceDirect
Journal of Sound and Vibration 318 (2008) 1077–1108
JOURNAL OF SOUND AND VIBRATION
www.elsevier.com/locate/jsvi

A statistical energy analysis subsystem formulation using finite element and periodic structure theory

V. Cotoni[a,*], R.S. Langley[b], P.J. Shorter[a]

[a]*ESI US R&D, 12555 High Bluff Drive, Suite 250, San Diego, CA 92130, USA*
[b]*Department of Engineering, University of Cambridge, Trumpington Street, Cambridge CB2 1PZ, UK*

Received 10 October 2006; received in revised form 28 April 2008; accepted 29 April 2008
Handling Editor: S. Bolton
Available online 26 July 2008

Abstract

In statistical energy analysis (SEA), a complex vibro-acoustic system is represented as an assembly of coupled subsystems. The parameters of an SEA model are typically derived by considering wave propagation within each subsystem. Analytical formulations exist for describing wave propagation in many commonly encountered subsystems (for example, flat plates, curved shells, ribbed panels, etc.). However, problematic subsystems are often encountered that are not well represented by existing analytical formulations. Examples include composite fuselages, isogrid fairings, complex ribbed panels and extruded train floors. This paper describes a SEA subsystem formulation based on a combination of finite elements (FEs), component mode synthesis (CMS) and periodic structure theory. The method enables the SEA parameters to be efficiently computed for very general structural panels. Expressions are derived for the modal density, damping loss factor and 'engineering units' response of the panel. By making use of an efficient Fourier transform approach, the resonant radiation efficiency, non-resonant transmission loss and acoustic input power are also obtained. The method is derived and a number of analytical and experimental validation cases are presented.

1. Introduction

1.1. Overview of SEA

Statistical energy analysis (SEA) represents a field of study in which statistical descriptions of a system are employed in order to simplify the analysis of complicated vibro-acoustic problems [1,2]. In SEA, a vibro-acoustic system is represented in terms of a collection of coupled subsystems that can receive, store, dissipate and transmit energy. The traditional approach to SEA modeling therefore typically involves (i) describing a complex system in terms of a number of simpler connected subsystems (with an emphasis on removing unnecessary detail in order to simplify an analysis) and (ii) finding the 'best fit' SEA subsystems from a fixed library of subsystem formulations. As noted by Smith [3], the general philosophy behind traditional SEA

*Corresponding author.
E-mail address: vincent.cotoni@esi-group-na.com (V. Cotoni).

0022-460X/$ - see front matter © 2008 Elsevier Ltd. All rights reserved.
doi:10.1016/j.jsv.2008.04.058

modeling is to remove complexity from an analysis and replace an analytically intractable problem by an equivalent problem that is analytically tractable.

In the wave approach to SEA, a subsystem is defined to be a collection of propagating wavetypes (sometimes referred to as a 'wavefield'). The analysis is simplified by assuming that the boundary conditions and/or lateral extent of the SEA subsystems are uncertain and drawn from a large ensemble of subsystems. The SEA parameters for a system can then be related to the properties of the propagating wavetypes of the various subsystems of a system. For example, the energy storage capacity (or modal density) of an SEA subsystem depends on (i) the average group velocity of the propagating waves within the subsystem and (ii) the overall dimension of the subsystem. The transmission of energy between subsystems depends on the coupling loss factors (CLFs) for a particular type of junction. Each CLF describes the power that is transmitted into the direct field of a receiving subsystem per unit (ensemble average) energy in the reverberant field of a source subsystem. The transmission of energy at a given junction depends on the impedance that each subsystem presents at a given type of connection. These impedances can, in turn, be determined from knowledge of the propagating and evanescent wavetypes within the subsystem. In summary, in order to describe a vibro-acoustic system using the wave approach to SEA it is necessary to determine (i) the wavetypes that can propagate within each subsystem (and, in particular, the dispersion information for each propagating wavetype) and (ii) the impedances that the subsystems present at a given type of connection.

It is possible to derive analytical expressions for the dispersion curves and impedances of subsystems that have simple cross-sections. Consider, for example, the thin flat plate with uniform cross-section shown in Fig. 1a. At low frequencies, the plate has three propagating wavetypes associated with extensional, shear and flexural waves. The dispersion curves for these wavetypes are relatively straightforward to derive and can be written in closed form (see Ref. [4] for example). Modern SEA codes typically contain extensive libraries of analytical algorithms for determining the dispersion curves and impedances of different types of subsystems. These algorithms can, for example, account for complex effects such as curvature, rib stiffening, internal pressurization and heavy fluid loading [5].

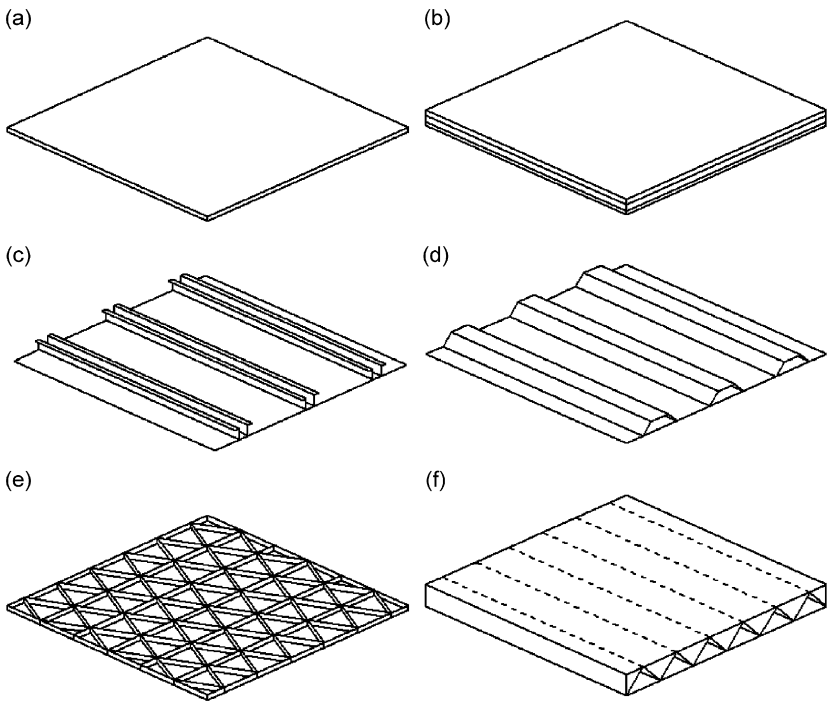

Fig. 1. Typical panel constructions: (a) simple uniform panel, (b) laminated panel, (c) skin-stringer fuselage, (d) corrugated composite fuselage, (e) isogrid launch vehicle fairing and (f) extruded aluminum train floor.

Using analytical expressions in the formulation of an SEA subsystem has the advantages that (i) the analytical expressions provide insights into the physical parameters that govern the response of the subsystem and (ii) the SEA parameters can be calculated with minimal computational effort. The disadvantage is that the formulations sometimes have a limited range of applicability. Consider, for example, the case of a general viscoelastic laminated section (as shown in Fig. 1b). Such sections are commonly encountered in laminated glasses and baked-on-mastics in the automotive industry, and in composite trim panels in the aerospace industry. Existing SEA formulations for uniform plates or simple sandwich panels are typically not generic enough to capture the physical response of such laminates. In order to create an accurate SEA model, it is therefore necessary to derive a new section formulation. For this problem, a generic SEA section formulation can be derived based on the use of spectral elements (for example, see Ref. [6]).

1.2. Problematic subsystems

Consider now the skin-stringer construction shown in Fig. 1c. This construction is often found in traditional aircraft fuselages (n.b., the effects of curvature are important for such constructions but are omitted from the figure for clarity). The stringers and frames of a traditional fuselage can often be approximated analytically as a set of orthogonal beams applied to a thin curved shell, making it possible to derive an analytical SEA formulation (see for example, Ref. [7]). Consider now the problem of describing the non-traditional corrugated fuselage construction shown in Fig. 1d. Such constructions are typically made from composite materials and are becoming increasingly common in modern aircraft fuselage designs. The 'stringers' in such constructions do not behave as simple beams, and it is therefore difficult to model such a construction using existing analytical SEA formulations.

A similar situation is encountered when modeling isogrid constructions in launch vehicle fairings. Isogrid constructions typically employ a periodic triangular arrangement of stiffeners as shown in Fig. 1e. The geometry and layout of the stiffeners are not particularly amenable to analysis using existing analytical SEA formulations. A further example is encountered when modeling the response of the extruded aluminum sections encountered in typical train floors (as shown in Fig. 1f). At low frequencies, the section typically behaves like an orthotropic panel, while at higher frequencies the individual corrugations start to exhibit localized behavior. Such constructions are, also, often difficult to model rigorously using existing analytical SEA formulations.

The previous examples highlight the need for the development of new, more general, SEA subsystem formulations. In principle, it might be possible to derive analytical models of wave propagation in such sections. However, the complexity of the derivation and resulting analytical expressions typically increases significantly as the section becomes more complex. It is therefore natural to question whether there is a generic way to derive a (two-dimensional (2D)) SEA subsystem formulation that (i) can account for an arbitrary amount of complexity in the subsystem construction, (ii) is robust and computationally efficient and (iii) can be used to accurately compute the required SEA parameters. The objective of this paper is to derive such a formulation.

In the following sections, a general method is proposed in which (i) a finite element (FE) model is created of a representative unit cell of the section, (ii) the computational expense of the FE model is reduced by performing component mode synthesis (CMS) on the unit cell, (iii) periodic boundary conditions are applied to the unit cell and the free propagating waves are obtained by solving an algebraic eigenvalue problem and (iv) various postprocessing expressions are developed in order to compute the required SEA properties for the section. The following analysis is therefore based on a 'wave approach' to SEA; similar results can be obtained using a 'modal approach' as reported in Appendix A.

1.3. Applications of periodic structure theory to SEA

Since the proposed method makes use of periodic structure theory it is useful to review applications of periodic structure theory to SEA. The analysis of wave propagation in periodic structures has been studied extensively over the past century (the text book by Brillouin [8] provides a detailed historical review). Mead

was among the first to apply periodic structure theory to the vibration of continuous systems [9] and presented a comprehensive review in Ref. [10]. While there is a significant amount of literature related to periodic structure theory, there are relatively few references that discuss the application of periodic structure theory to SEA.

Keane and Price [11] studied the use of periodic structure theory in the context of SEA. Their analysis was primarily concerned with refining various statistical assumptions in the modal approach to SEA, using information from an analytical periodic structure model. As noted by Keane and Price, the response of a slightly disordered periodic structure can sometimes be different to that of a perfectly periodic structure. This point is relevant for the current work, and the effects of irregularity on wave propagation through weakly coupled periodic systems should also, ideally, be investigated. The assumption of a perfectly periodic section is, however, likely to be adequate for the subsystems encountered in typical SEA applications.

Langley [12] discussed the calculation of the modal density of various one and 2D structures using periodic structure theory. Various expressions were obtained for the energy flow within the periodic structures. The approach was primarily concerned with the evaluation of modal density and expressions for other SEA parameters were not presented explicitly. The transmission of energy between two SEA plates coupled by a deterministic periodic plate was discussed by Langley et al. [13]. In this approach, the periodic plate is effectively a deterministic 'junction' between the two SEA subsystems (and is not an SEA subsystem itself). Tso and Hansen [14] discussed the calculation of the wave transmission coefficient between two semi-infinite plates, one of which is represented using one-dimensional (1D) periodic structure theory. While this approach predicts the transmission into the receiving periodic subsystem, the analysis is restricted to a particular class of periodic structures. The analysis is also mainly concerned with the wave transmission coefficient into the receiving subsystem and does not consider the calculation of other SEA parameters.

Finnveden [15] discusses an alternative approach to modeling the response of a 1D waveguide using a 2D spectral element formulation. In this approach, the displacement field across the cross-section of the waveguide is described using a series of 2D FEs, while the displacement field along the waveguide is described analytically. The wavetypes can then be obtained by solving an algebraic eigenvalue problem. 2D spectral element approaches have the advantage that they can be applied to 1D waveguides with arbitrarily complex cross-sections. Such models can be used to compute SEA properties for plate and shell structures. However, this approach implicitly assumes that the cross-section of the waveguide is known deterministically (and that uncertainty only exists in the length of the waveguide). Such approaches are therefore typically better suited to modeling 1D components such as beams and ducts in an SEA context. Furthermore, a 2D spectral element approach cannot be easily applied to problems in which the periodicity is truly 2D (for example the isogrid structure shown in Fig. 1e).

The previous references are mainly concerned with periodicity in structural components. In the current paper, interest lies not only in the vibrational response of a 2D periodic structure but also in the interactions between the structure and surrounding acoustic media (in particular, acoustic radiation and acoustic transmission loss). The remaining sections of the papers are organized as follows. The periodic theory is briefly reviewed in Section 2. The use of CMS is then proposed in order to reduce the computational expense of the approach. The derivation of various subsystem properties (modal density, damping and 'engineering units' data recovery), are described in Section 3. Section 4 discusses the calculation of the power input from pressure loads, and the radiation efficiency and transmission loss of the section. Finally, a number of validation examples are presented in Section 5. Appendix A describes an alternative 'modal approach' to derive the same properties.

2. Periodic structure theory

2.1. Review of standard approach

The current work adopts the periodic theory developed in Ref. [16] for 2D structures. The approach is briefly summarized in this section. Consider a general structure with 2D periodicity. A periodic *cell* can be

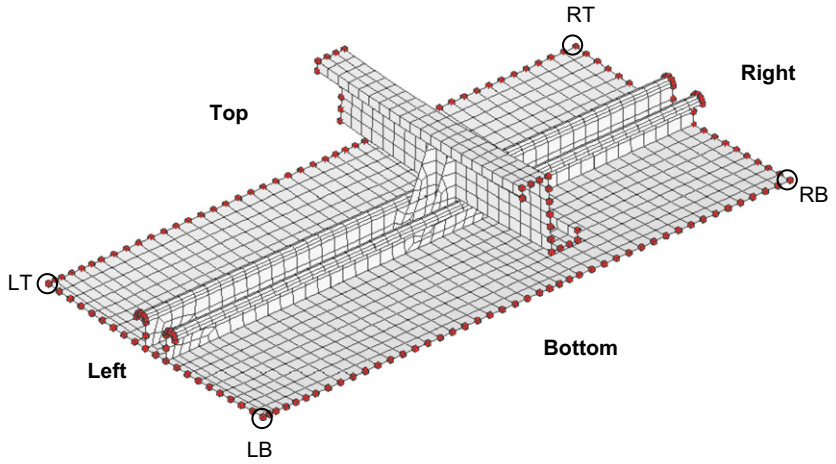

Fig. 2. Labeling of edge and corner degrees of freedom for a unit cell of a general 2D periodic structure.

extracted from the structure and modeled using a FE model with degrees of freedom $\mathbf{q}$, as shown in Fig. 2. Steady-state harmonic vibration of frequency ω is considered in what follows and all response quantities are represented by complex amplitudes so that $\mathbf{q}$, for example, corresponds to the time-dependent response $\mathbf{q}(t) = \mathrm{Re}\{\mathbf{q}\, e^{i\omega t}\}$. The degrees of freedom $\mathbf{q}$ of the cell can be partitioned into interior (I), edge (L, R, B, T) and corner (LB, RB, LT and RT) degrees of freedom. The internal degrees of freedom are not connected to other periodic cells.

The vibration response of the structure at a given frequency can be analyzed by specifying a phase lag between the displacement degrees of freedom at the left, right, bottom and top edges so that

$$\mathbf{q}_R = e^{-i\varepsilon_x}\mathbf{q}_L, \quad \mathbf{q}_T = e^{-i\varepsilon_y}\mathbf{q}_B. \tag{1}$$

Similarly, the response of the corner degrees of freedoms may be expressed in terms of the left-bottom corner response as

$$\mathbf{q}_{\mathrm{RB}} = e^{-i\varepsilon_x}\mathbf{q}_{\mathrm{LB}}, \quad \mathbf{q}_{\mathrm{LT}} = e^{-i\varepsilon_y}\mathbf{q}_{\mathrm{LB}}, \quad \mathbf{q}_{\mathrm{RT}} = e^{-i\varepsilon_x - i\varepsilon_y}\mathbf{q}_{\mathrm{LB}}. \tag{2}$$

The terms ε_x and ε_y are referred to as 'phase constants.' For free wave propagation in an undamped structure these constants are real and can take values between $-\pi$ and π.

In the current analysis, the unit cell is described with FEs so that the degrees of freedom refer to nodal displacements and rotations. In order to apply periodic boundary conditions, it is therefore necessary to ensure that the node locations on opposite edges and corners of the cell are identical. The following analysis is not restricted to 'flat' periodic structures and can also be applied to curved structures. For such structures, it is important to ensure that the edge and corner degrees of freedom are defined in the appropriate local coordinate system. If all degrees of freedom are initially expressed in the global coordinate system, then a simple rotation matrix can be used to convert from the global system into the local rotated coordinates.

The complete vector of local degrees of freedom of the cell can be ordered so that

$$\mathbf{q} = \left[\mathbf{q}_I^{\mathrm{T}} \,|\, \mathbf{q}_B^{\mathrm{T}} \quad \mathbf{q}_T^{\mathrm{T}} \quad \mathbf{q}_L^{\mathrm{T}} \quad \mathbf{q}_R^{\mathrm{T}} \,|\, \mathbf{q}_{\mathrm{LB}}^{\mathrm{T}} \quad \mathbf{q}_{\mathrm{RB}}^{\mathrm{T}} \quad \mathbf{q}_{\mathrm{LT}}^{\mathrm{T}} \quad \mathbf{q}_{\mathrm{RT}}^{\mathrm{T}}\right]^{\mathrm{T}}. \tag{3}$$

The undamped equation of motion for the cell is given by

$$[\mathbf{K} - \omega^2\mathbf{M}]\mathbf{q} = \mathbf{F}, \tag{4}$$

where $\mathbf{M}$ and $\mathbf{K}$ are the nodal mass and stiffness matrices for the unit cell and $\mathbf{F}$ is the generalized force vector. The propagation relations in Eqs. (1) and (2) can be written in matrix form as

$$\mathbf{q}' = \mathbf{R}\mathbf{q} \quad \text{with} \quad \mathbf{R} = \left[\begin{array}{cccc} \mathbf{I} & \mathbf{0} & \mathbf{0} & \mathbf{0} \\ \hline \mathbf{0} & \mathbf{I} & \mathbf{0} & \mathbf{0} \\ \mathbf{0} & \mathbf{I}e^{-i\varepsilon_y} & \mathbf{0} & \mathbf{0} \\ \mathbf{0} & \mathbf{0} & \mathbf{I} & \mathbf{0} \\ \mathbf{0} & \mathbf{0} & \mathbf{I}e^{-i\varepsilon_x} & \mathbf{0} \\ \hline \mathbf{0} & \mathbf{0} & \mathbf{0} & \mathbf{I} \\ \mathbf{0} & \mathbf{0} & \mathbf{0} & \mathbf{I}e^{-i\varepsilon_x} \\ \mathbf{0} & \mathbf{0} & \mathbf{0} & \mathbf{I}e^{-i\varepsilon_y} \\ \mathbf{0} & \mathbf{0} & \mathbf{0} & \mathbf{I}e^{-i\varepsilon_x - i\varepsilon_y} \end{array}\right], \tag{5}$$

where $\mathbf{q}' = [\mathbf{q}_I\ \mathbf{q}_B\ \mathbf{q}_L\ \mathbf{q}_{\mathrm{LB}}]^{\mathrm{T}}$. The previous expression can be used to reduce various degrees of freedom from Eq. (4). The resulting homogenous equation in the reduced set of coordinates is then given by

$$[\mathbf{K}' - \omega^2\mathbf{M}']\mathbf{q}' = 0, \tag{6}$$

where

$$\mathbf{K}' = \mathbf{R}^{\mathrm{H}}(\varepsilon_x, \varepsilon_y)\mathbf{K}\mathbf{R}(\varepsilon_x, \varepsilon_y), \quad \mathbf{M}' = \mathbf{R}^{\mathrm{H}}(\varepsilon_x, \varepsilon_y)\mathbf{M}\mathbf{R}(\varepsilon_x, \varepsilon_y), \tag{7}$$

and where $\mathbf{R}^{\mathrm{H}}$ denotes the complex conjugate (or Hermitian) transpose of $\mathbf{R}$. If a particular set of phase constants $(\varepsilon_x,\varepsilon_y)$ are specified then the previous expression represents a standard eigenvalue problem. If $\mathbf{K}$ and $\mathbf{M}$ are real symmetric then $\mathbf{M}'$ and $\mathbf{K}'$ are Hermitian and the resulting eigenvalues are real and the eigenvectors are complex. The eigenvalues Ω_n^2 indicate the frequencies at which a wave can propagate in the structure when a particular phase lag is specified between the edge and corner degrees of freedom. The eigenvectors $\boldsymbol{\varphi}_n$ describe the corresponding motion of the periodic cell. The eigenvectors can be mass normalized so that $\boldsymbol{\varphi}_n{}^{\mathrm{H}}\mathbf{M}'\boldsymbol{\varphi}_n = 1$.

Many eigenvalues arise for a given set of phase constants since (i) several waves can propagate under a given periodic constraint and (ii) the periodicity condition is defined modulo 2π. The function $\Omega_n(\varepsilon_x,\varepsilon_y)$ can be plotted for each eigenvalue; the resulting plots are typically referred to as 'phase constant surfaces.' Fig. 3 shows an example of a plot of the phase constant surfaces for a typical periodic cell.

If the unit cell exhibits symmetry then there is also symmetry in the phase constant surfaces. This can be used to reduce computational expense when computing the phase constant surfaces. For example, the eigensolution for $(-\varepsilon_x, -\varepsilon_y)$ is identical to the solution for $(\varepsilon_x,\varepsilon_y)$ because of the symmetry of the equations when the propagation direction is reversed. For orthotropic structures, it is also possible to further reduce the range to $0<\varepsilon_x<\pi$. Further reductions in computational expense can be obtained by truncating the number of phase surfaces considered in a given analysis. In the current analysis, only the solutions with eigenvalue $\Omega(\varepsilon_x,\varepsilon_y)$ in a given frequency range are extracted (this is similar to the truncation of the modal series in a standard modal analysis).

In principle, the eigenvalues of Eq. (6) can be directly calculated for a given set of phase constants. In practice, it is often found that the repeated solution of this eigenvalue problem can be computationally expensive for problems in which the unit cell has a moderately large number of degrees of freedom. Significant savings in computational expense can be obtained by reducing the number of degrees of freedom used to describe the response of the unit cell. The following section therefore discusses the use of CMS to reduce the computational expense associated with determining the phase constant surfaces for a given unit cell.

2.2. CMS

CMS is a standard method for reducing the size of a large FE model by describing the global response in terms of the component modes of various local substructures [17]. The use of fixed interface

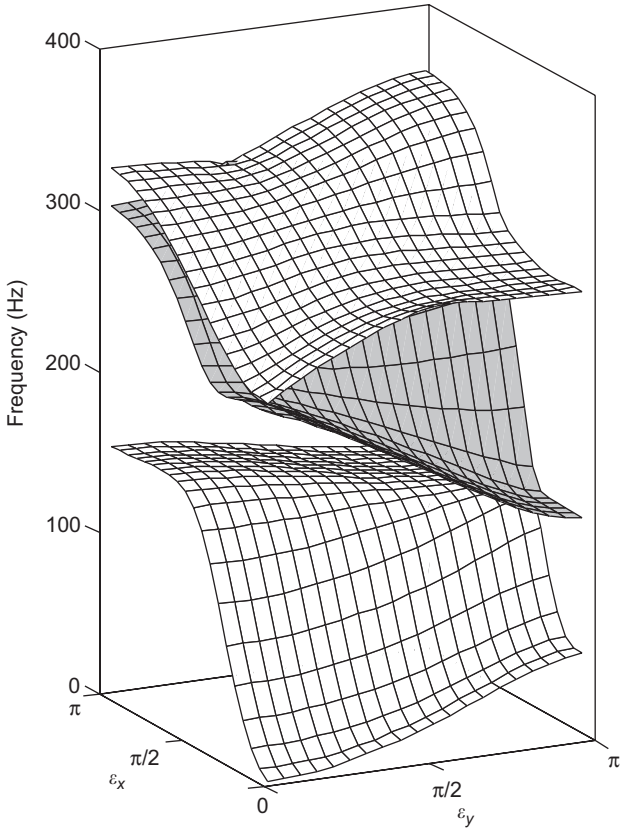

Fig. 3. The first three phase constant surfaces for a cross-wise stiffened flat panel.

(or Craig–Bampton) CMS is particularly well suited for periodic structure theory since the edge degrees of freedom are retained as separate degrees of freedom in the analysis. In fixed interface CMS, the response of a system is represented in terms of a set of 'component' modes and 'constraint' modes. The component modes $\mathbf{\Phi}$ are taken to be a subset of the local modes of a substructure when the boundary degrees of freedom are clamped. The constraint modes are given by the static response of the substructure when a unit displacement or rotation is applied to a given boundary degree of freedom while all other boundary degrees of freedom remain fixed.

The degrees of freedom in Eq. (4) can be partitioned into the set of interior degrees of freedom $\mathbf{q}_I$ and a set of boundary (edge and corner) degrees of freedom $\mathbf{q}_b$ so that $\mathbf{q} = [\,\mathbf{q}_I^{\mathrm{T}} \quad \mathbf{q}_b^{\mathrm{T}}\,]^{\mathrm{T}}$. A reduced set of degrees of freedom $\mathbf{p}$ is then defined so that $\mathbf{p} = [\,\mathbf{q}_\phi^{\mathrm{T}} \quad \mathbf{q}_b^{\mathrm{T}}\,]^{\mathrm{T}}$ where $\mathbf{q}_\phi$ represents the amplitudes of the fixed interface component modes. The nodal degrees of freedom $\mathbf{q}$ are related to the component modal degrees of freedom $\mathbf{p}$ by the following transformation:

$$\mathbf{q} = \mathbf{C}\mathbf{p}, \quad \mathbf{C} = \begin{bmatrix} \mathbf{\Phi} & -\mathbf{K}_{II}^{-1}\mathbf{K}_{Ib} \\ \mathbf{0} & \mathbf{I} \end{bmatrix}. \tag{8}$$

It can be seen that the edge and corner degrees of freedom are retained in the analysis; the CMS reduction provides an efficient basis with which to describe the response of the interior degrees of freedom. Converged results can typically be obtained by retaining component modes with natural frequencies less than twice the maximum frequency in the analysis. The number of component modal degrees of freedom is therefore typically much smaller than the number of original degrees of freedom of the unit cell.

If the component modes are mass normalized, then the reduced mass and stiffness matrices are given by

$$\mathbf{M}^r = \mathbf{C}^{\mathrm{T}}\mathbf{M}\mathbf{C} = \begin{bmatrix} \mathbf{I} & \mathbf{M}^r_{\phi b} \\ \mathbf{M}^r_{b\phi} & \mathbf{M}^r_{bb} \end{bmatrix} \quad \text{and} \quad \mathbf{K}^r = \mathbf{C}^{\mathrm{T}}\mathbf{K}\mathbf{C} = \begin{bmatrix} \boldsymbol{\lambda} & \mathbf{0} \\ \mathbf{0} & \mathbf{K}^r_{bb} \end{bmatrix}, \tag{9}$$

where $\boldsymbol{\lambda}$ is a diagonal matrix which contains the squared circular natural frequencies for the component modes.

One of the advantages of using CMS in the context of the periodic equations is that the reduction only needs to be performed once (and does not have to be re-evaluated for each value of the phase constants). This therefore leads to a significant reduction in computational expense. For problems involving a moderate number of interior degrees of freedom, the authors have observed speedups of approximately $100\times$ using CMS (with a negligible impact on the accuracy of the results).

3. Subsystem properties

In this section, it is shown that the SEA parameters for a given structure can be related to certain properties of the phase surfaces of a unit cell. A 'diffuse reverberant field' in the structure is represented as an incoherent addition of the waves in a given frequency band of interest. Expressions for the modal density, damping loss factor and engineering units response are then obtained in terms of various integrations in 'phase' space.

The following assumptions are made in this section: (i) it is assumed that the dispersion curves of the propagating waves are not significantly modified by the addition of damping (i.e. the propagating waves obtained from Eq. (6) can be used to represent the damped response); (ii) all wavetypes within a section are assumed to be in equipartition of energy (i.e. no attempt is made to classify individual wavetypes, for example, bending, shear and longitudinal waves in a panel) and (iii) the reactive impedance of any adjacent fluids is negligible so that the dispersion curves of the propagating waves of the structure are not significantly modified by the addition of an adjacent fluid (i.e. the propagating waves obtained from Eq. (6) can be used to represent the coupled response).

3.1. Modal density

It is shown in Ref. [12] that the modal density of a periodic structure with $N_x \times N_y$ cells can be obtained by computing the area of the phase constant surfaces lying below the frequency ω so that

$$n(\omega) = \frac{\partial N}{\partial \omega}, \quad \text{where } N(\omega) = \frac{N_x N_y}{4\pi^2} \sum_n \left(\int_{-\pi}^{\pi} \int_{-\pi}^{\pi} H(\omega - \Omega_n(\varepsilon_x, \varepsilon_y)) \, \mathrm{d}\varepsilon_x \, \mathrm{d}\varepsilon_y \right), \tag{10}$$

and where the Heaviside step function H is given by $H(x<0)=0$, $H(x>0)=1$. The summation n in the previous expression runs over the phase constant surfaces (i.e. the eigensolutions associated with each $(\varepsilon_x,\varepsilon_y)$ pair).

The previous expression describes the modal density in terms of an integration in 'phase space.' The following section presents an alternative derivation of the modal density in terms of an integration in 'wavenumber space.' For planar structures aligned with the x–y plane there is a direct correspondence between phase space and wavenumber space. For example, the displacement field associated with wave propagation in a planar structure can be written as $\varphi(x,y,z) = \varphi(z)\mathrm{e}^{-\mathrm{i}(k_x x + k_y y)}$, where the wavenumbers k_x and k_y are related to the phase constants via the congruence relations $\varepsilon_x \equiv k_x l_x \, mod \, 2\pi$, $\varepsilon_y \equiv k_y l_y \, mod \, 2\pi$. The dispersion curves $k_x(\omega)$ and $k_y(\omega)$ associated with a given propagating wave can therefore be obtained by 'unwrapping' the solutions of Eq. (6) in phase space. This then provides an alternative method for computing the modal density of a given wavetype. The modal density of the nth wavetype can be expressed in terms of the following integral along a given dispersion curve k_n in wavenumber space [12]:

$$n_n(\omega) = \frac{A_N}{(2\pi)^2} \int_0^{2\pi} k_n(\theta,\omega) \left| \frac{\partial k_n(\theta,\omega)}{\partial \omega} \right| \mathrm{d}\theta, \tag{11}$$

where $A_N = N_x N_y A$ is the effective surface area of the complete periodic structure made of $N_x \times N_y$ cells of area A, and the wavenumber is expressed in polar coordinates. The derivative inside the integral could be evaluated numerically from the calculation of the wavenumber $k_n(\theta,\omega)$ at two closely separated frequencies. However, a more efficient way to proceed is to use the matrix relations recently proposed by Finnveden [15] for waveguides.

The matrix $\mathbf{R}$ in Eq. (5) can be expressed in polar coordinates in terms of the modulus and heading of the phase constants, that is $\mathbf{R}(k_n,\theta_n)$. Let $\mathbf{D}$ denote the dynamic stiffness matrix of the cell, $\mathbf{D}(\omega) = \mathbf{K} - \omega^2\mathbf{M}$. Consider a solution $(\Omega_n, \boldsymbol{\varphi}_n)$ of Eq. (6). Differentiating Eq. (6) with respect to k_n at the frequency Ω_n yields

$$\left(\frac{\partial \mathbf{R}^{\mathrm{H}}}{\partial k_n}\mathbf{D}(\Omega_n)\mathbf{R} + \mathbf{R}^{\mathrm{H}}\mathbf{D}(\Omega_n)\frac{\partial \mathbf{R}}{\partial k_n} - 2\Omega_n\frac{\partial \omega}{\partial k_n}\mathbf{R}^{\mathrm{H}}\mathbf{M}\mathbf{R}\right)\boldsymbol{\varphi}_n + (\mathbf{R}^{\mathrm{H}}\mathbf{D}(\Omega_n)\mathbf{R})\frac{\partial \boldsymbol{\varphi}_n}{\partial k_n} = \mathbf{0}, \tag{12}$$

where the $\mathbf{R}$ matrices are evaluated at (k_n,θ_n). Given that the matrices in Eq. (6) are Hermitian, pre-multiplying Eq. (12) by the conjugate transpose of the eigenvector $(\boldsymbol{\varphi}_n)^{\mathrm{H}}$ removes the second term in parentheses. The frequency derivative of the wavenumber (at the frequency Ω_n) is then given by

$$\frac{\partial k_n}{\partial \omega}(\Omega_n) = \frac{2\Omega_n}{\boldsymbol{\varphi}_n^{\mathrm{H}}((\partial \mathbf{R}^{\mathrm{H}}/\partial k_n)\mathbf{D}(\Omega_n)\mathbf{R} + \mathbf{R}^{\mathrm{H}}\mathbf{D}(\Omega_n)(\partial \mathbf{R}/\partial k_n))\boldsymbol{\varphi}_n}, \tag{13}$$

where it has been noted that the eigenvectors are mass normalized so that $\boldsymbol{\varphi}_n^{\mathrm{H}}(\mathbf{R}^{\mathrm{H}}\mathbf{M}\mathbf{R})\boldsymbol{\varphi}_n = 1$. It is shown in Refs. [12,15] that Eq. (13) can be singular at the cut-on frequencies of the waves (or equivalently at the bounds of the pass bands). The integral over wavenumber space, remains finite however.

In summary, if the unwrapped wavenumbers can be computed (using, for example, root tracking algorithms) then Eqs. (11) and (13) provide an alternative method for evaluating the modal density of a given wavetype using a wavenumber approach.

3.2. Damping loss factor

The previous analysis assumed that the structure was undamped. Suppose now that damping is introduced into the structure by specifying a damping loss factor $\eta(\mathbf{x},\omega)$, which varies with frequency and position within the unit cell. The damping distribution may, for example, be used to describe a polymer layer in a viscoelastic laminate or a local damping treatment applied to an aerospace fuselage. Typically, in an SEA analysis, an overall subsystem damping loss factor $\eta_s(\omega)$ is defined. This subsystem damping loss factor describes the overall (ensemble average) power dissipated by the subsystem when a diffuse reverberant field exists within the subsystem. If the damping is spatially uniform then $\eta_s = \eta$. If the damping is not spatially uniform then η_s becomes a function of the phase constant surfaces and the damping distribution $\eta(\mathbf{x},\omega)$, as discussed in the following section.

The damping loss factor associated with a particular propagating wave in the structure is given by Ref. [6]: $\eta_n(\varepsilon_x, \varepsilon_y) = P_{\mathrm{diss}}/\omega E$, where P_{diss} is the power dissipated by the section and E is the energy of the section. The dissipated power and energy are functions of the phase constants $(\varepsilon_x,\varepsilon_y)$ and eigensolution number n. In the following analysis, structural damping (or 'complex stiffness') is assumed so that the dissipated power is proportional to the local strain energy. Suppose that different local damping loss factors η_r are applied to various regions of the structure. The dissipated power can then be written as

$$P_{\mathrm{diss}} = \sum_r 2\omega\eta_r U_r, \tag{14}$$

where U_r is the strain energy associated with the region with damping loss factor η_r. The strain and total energies can be expressed in terms of the corresponding FE mass and stiffness matrices and the wave displacement shape (or eigenvector) $\boldsymbol{\varphi}_n(\varepsilon_x,\varepsilon_y)$, so that

$$\eta_n(\varepsilon_x, \varepsilon_y) = \frac{\sum_r 2\eta_r \boldsymbol{\varphi}_n^{\mathrm{H}}(\mathbf{R}^{\mathrm{H}}\mathbf{K}_r\mathbf{R})\boldsymbol{\varphi}_n}{\boldsymbol{\varphi}_n^{\mathrm{H}}[\omega^2\mathbf{M}' + \mathbf{K}']\boldsymbol{\varphi}_n}, \tag{15}$$

where $\mathbf{K}_r$ is the contribution of the rth region to the total stiffness matrix of the unit cell. The matrices $\mathbf{R}$, $\mathbf{M}'$ and $\mathbf{K}'$ and the eigenvector $\boldsymbol{\varphi}_n$ in Eq. (15) are functions of the phase constants $(\varepsilon_x,\varepsilon_y)$. Suppose now that a

diffuse reverberant field exists within the subsystem. A diffuse reverberant field can be interpreted as being the field obtained from the incoherent addition of all 'resonant' wavetypes contained within a given frequency band of interest and carrying the same energy. From a wave approach, the section damping loss factor can therefore be obtained by averaging the previous expression over all values of the phase constants whose natural frequencies lie within a given frequency band of interest $\Delta\omega$.

The time-average energy of the periodic structure associated with the wave displacement field $\boldsymbol{\varphi}_n(\varepsilon_x,\varepsilon_y)$ is given by

$$E_n(\varepsilon_x,\varepsilon_y)=\frac{N_xN_y}{4}\boldsymbol{\varphi}_n^{\mathrm{H}}[\omega^2\mathbf{M}'+\mathbf{K}']\boldsymbol{\varphi}_n=\frac{N_xN_y}{4}(\omega^2+\Omega_n^2(\varepsilon_x,\varepsilon_y)). \tag{16}$$

When the wave is resonant, $\omega=\Omega_n$, and the energy therefore reduces to $N_xN_y\omega^2/2$. It can be seen that the resonant waves (obtained with the adopted mass normalization scheme) have the same energy. The average resonant damping is therefore given by

$$\eta_s(\omega)=\left\langle \eta_n(\varepsilon_x,\varepsilon_y)\right\rangle_{\varepsilon_x,\varepsilon_y,n/\Omega_n(\varepsilon_x,\varepsilon_y)\in\Delta\omega}, \tag{17}$$

where $\langle\ \rangle$ denotes the average and $\eta_n(\varepsilon_x,\varepsilon_y)$ is given by Eq. (15).

3.3. Engineering units data recovery

The primary outputs of an SEA calculation are the (ensemble average) subsystem energies, and the powers exchanged between subsystems. The 'engineering units' response of a subsystem (i.e. the velocity response for structural subsystems and/or the pressure response for acoustics subsystems) can be found by postprocessing the subsystem energies. The engineering units response of a given subsystem can, in principle, be found by adding the ensemble average 'reverberant' response of the subsystem and the 'direct fields' from any connections to the subsystem. In practice, for lightly damped subsystems, the reverberant fields of the subsystems tend to be dominant and the direct fields are typically neglected. Simplified expressions are then typically used to relate the engineering units response to the subsystem resonant energies. For example, for spatially homogeneous structural subsystems the time-average total resonant energy is given by $E=M\overline{v^2}$ [1], where M is the mass of the subsystem and $\overline{v^2}$ is the space-average mean square resonant velocity (i.e. half the space averaged modulus square velocity).

For more complex subsystems, there can be significant spatial variations in the engineering units response when a diffuse reverberant field exists within the subsystem. Consider, for example, a diffuse reverberant field within a ribbed panel subsystem; at higher frequencies, the response on the skin is typically much higher than the response on the ribs. For a complex periodic structure, it is possible to derive expressions for the spatial variations in the engineering units response as discussed in the following section.

As discussed previously, a diffuse reverberant field can be interpreted as an incoherent addition of the wavetypes in a given frequency band of interest. The time-average energy associated with a resonant wave was shown to be $N_xN_y\omega^2/2$. The cross-spectral velocity matrix associated with the wave displacement field $\boldsymbol{\varphi}_n(\varepsilon_x,\varepsilon_y)$ in a cell is given by $\omega^2\boldsymbol{\varphi}_n\boldsymbol{\varphi}_n{}^{\mathrm{H}}$. Averaging over all resonant waves in a given frequency band gives the following relationship between the engineering units response of the subsystem and the ensemble average subsystem energy E:

$$(\mathbf{S}_{vv})=\frac{2E}{N_xN_y}\left\langle\boldsymbol{\varphi}_n\boldsymbol{\varphi}_n^{\mathrm{H}}\right\rangle_{\varepsilon_x,\varepsilon_y,n/\Omega_n(\varepsilon_x,\varepsilon_y)\in\Delta\omega}. \tag{18}$$

The cross-spectral velocity matrix in Eq. (18) is for response locations in the same periodic cell (the phase constant lag can be included to describe the cross-spectrum of points in different cells). The modulus square velocity at each node can be obtained from the diagonal entries of the cross-spectral velocity matrix.

4. Coupling with acoustics

The previous sections have discussed the calculation of the response of the structure *in vacuo*. Suppose now that the 'front' and/or 'back' of the structure are 'wetted' by adjacent fluids. In an SEA model, the coupling

between the structure and the fluids can be described by (i) CLFs between the resonant modes of the panel and the adjacent fluids, (ii) an indirect (or non-resonant) CLF between the two fluids and (iii) an input power to the resonant modes of the panel from an arbitrary blocked pressure loading within either fluid (due to, for example, the presence of turbulent boundary layer excitation within the fluid). In this section, the average resonant radiation efficiency, the power input from a distributed pressure loading, and the non-resonant acoustic transmission are computed from the eigensolutions of Eq. (6).

Consider a periodic structure that is coupled to a fluid across a finite rectangular 'connection region' of dimension $N_x \times N_y$ cells. It is assumed in what follows that a continuous coupling surface (or 'wetted' face) can be defined over the connection region when the 'wetted' face associated with the periodic cell is repeated in the two directions of periodicity. For example, in the structure shown in Fig. 2, the wetted face can be taken to be the 'skin' of the cell.[1] In the following analysis, the normal component of the wave displacement shape $\boldsymbol{\varphi}$ is obtained and projected onto the wetted surface of the unit cell. The resulting displacement is represented by the scalar field $\varphi(x, y)$. A spatial Fourier transform is then performed across the unit cell. The Fourier transform for the connection region is related to the Fourier transform across the unit cell as discussed in the following section.

4.1. Wavenumber transform and periodic structures

A local Cartesian coordinate system (x, y) is defined across the wetted surface of the unit cell and a global Cartesian coordinate system (X, Y) is defined across the wetted surface of the larger connection region. The dimensions of the unit cell can be denoted by l_x and l_y. The mapping between the global and local coordinates for cell $\mathbf{r} = (r_x, r_y)$ within the structure is given by $X = x + r_x l_x$, $Y = y + r_y l_y$. The displacement (or pressure) field associated with phase constants $(\varepsilon_x, \varepsilon_y)$ over the cell $\mathbf{r}$ can be written in terms of the field u across the unit cell as [18]

$$u(X, Y) = u(x, y)\mathrm{e}^{-\mathrm{i}r_x\varepsilon_x - \mathrm{i}r_y\varepsilon_y}. \tag{19}$$

Suppose now that the connection region is placed inside a rigid baffle, so that the displacement field outside of the connection region is zero. The spatial Fourier transform of the displacement field can then be written as [19]

$$\tilde{U}(k_x, k_y) = \iint_{A_N} u(X, Y)\mathrm{e}^{-\mathrm{i}(k_x X + k_y Y)}\,\mathrm{d}X\,\mathrm{d}Y, \tag{20}$$

where A_N denotes the surface area of the connection region, and the tilde ($\tilde{}$) indicates that the wavenumber transform is associated with the field defined over the entire connection region. Eq. (19) can be inserted into Eq. (20), and the integral over the whole connection region can be separated into $N_x N_y$ integrals over the cells of area A. Changing the integration variables from global to local then gives

$$\tilde{U}(k_x, k_y) = \left(\iint_{A} u(x, y)\mathrm{e}^{-\mathrm{i}(k_x x + k_y y)}\,\mathrm{d}x\,\mathrm{d}y \right) \sum_{r_x=0}^{N_x-1} \sum_{r_y=0}^{N_y-1} \mathrm{e}^{-\mathrm{i}\left(r_x(\varepsilon_x + k_x l_x) + r_y(\varepsilon_y + k_y l_y)\right)}. \tag{21}$$

The first term is the Fourier transform of the displacement field over the unit cell (noted U without tilde). The double summation over r_x and r_y can be expressed in closed form. In the following sections, the modulus square Fourier transform is used. This Fourier transform is related to the Fourier transform over the unit cell by the following expression:

$$|\tilde{U}(k_x, k_y)|^2 = |U(k_x, k_y)|^2 \kappa(N_x, \varepsilon_x + k_x l_x)\kappa(N_y, \varepsilon_y + k_y l_y) \quad \text{with} \quad \kappa(N, \varepsilon) = \frac{1 - \cos(N\varepsilon)}{1 - \cos(\varepsilon)}. \tag{22}$$

[1] For a typical ribbed panel, the direct acoustic coupling of the ribs is often small since (i) the ribs usually undergo less motion than the skin, (ii) their surface area is typically small when compared with the skin, and (iii) both sides of the ribs radiate in the fluid, making them inefficient dipole-like radiators over much of the frequency range of interest.

The function κ can be viewed as accounting for the finite size and periodicity of the connection region, and relates the wavenumber content across the connection region to the wavenumber content of the unit cell. The function peaks at $\varepsilon = 2\pi n$ with n an integer, and the magnitude of each peak is N^2. As the size of the structure extends to infinity, the function κ becomes a series of delta functions, so that $\kappa(\infty, \varepsilon) = 4\pi^2/l \sum_{n=-\infty}^{\infty} \delta(\varepsilon + 2\pi n)$.

4.2. Acoustic radiation

This section describes the calculation of the resonant radiation efficiency of the structure. The radiation efficiency of a given wetted face can be defined in terms of the acoustic power radiated Π, and the space-average mean square velocity $\overline{v^2}$, as $\sigma_{\text{rad}} = \Pi/(\rho c A_N \overline{v^2})$, where ρ and c are the fluid density and speed of sound and A_N the wetted surface area [4,20]. In an SEA model, interest lies in predicting the (ensemble average) radiation efficiency when a diffuse reverberant field exists within the subsystem. In the following analysis, a wave approach is adopted and the average mean square velocity and the radiated power are found from the incoherent contributions of all *in-vacuo* waves that are 'resonant' in a given frequency band of interest.

The mean square velocity associated with a particular wave displacement shape $\boldsymbol{\varphi}_n(\varepsilon_x,\varepsilon_y)$ can be found by integrating the displacement field φ_n across the wetted surface of the connection region:

$$\overline{v^2}_n(\varepsilon_x, \varepsilon_y) = \frac{\omega^2}{2A_N} \iint_{A_N} |\varphi_n(X, Y)|^2 \, \mathrm{d}X \, \mathrm{d}Y. \tag{23}$$

The time-average acoustic power radiated by the wave displacement shape $\boldsymbol{\varphi}_n(\varepsilon_x,\varepsilon_y)$ is given by the surface integral of the product $1/2\ \mathrm{Re}\{\mathrm{i}\omega\varphi_n p_n^*\}$, where p_n is the surface pressure induced by the displacement field φ_n. If the wetted surface is approximately planar, then the radiated pressure can be written using Rayleigh's integral [20], so that

$$p_n(X, Y) = \iint_{A_N} \varphi_n(X', Y') g(X - X', Y - Y', \omega) \, \mathrm{d}X' \, \mathrm{d}Y', \tag{24}$$

where the free-field Green's function of an (untrimmed) baffled structure is given by $g(X - X', Y - Y', \omega) = \rho\omega^2 \, \mathrm{e}^{-\mathrm{i}kR}/2\pi R$, with R the distance between the points (X,Y) and (X',Y'), ρ the fluid density, and k the acoustic wavenumber. Multiplying Eq. (24) by the velocity field and integrating over the wetted surface gives

$$\Pi_n(\varepsilon_x, \varepsilon_y) = \frac{1}{2} \mathrm{Re} \left\{ \iint_{A_N} \iint_{A_N} \mathrm{i}\omega \varphi_n(X', Y') \varphi_n^*(X', Y') g^*(X - X', Y - Y', \omega) \, \mathrm{d}X' \, \mathrm{d}Y' \, \mathrm{d}X \, \mathrm{d}Y \right\}. \tag{25}$$

The Green's function can be expressed in terms of its wavenumber transform, $G(k_x, k_y, \omega) = \mathrm{i}\rho\omega^2/(k^2 - k_x^2 - k_y^2)^{1/2}$ [19]. By inverting the order of the wavenumber and spatial integrals, the radiated power can be written in term of the wavenumber transform $\tilde{\phi}_n$ of the wave field over the connection region:

$$\Pi_n(\varepsilon_x, \varepsilon_y) = \frac{\omega}{8\pi^2} \int_{-\infty}^{\infty} \int_{-\infty}^{\infty} \mathrm{Im}\{G(k_x, k_y, \omega)\} |\tilde{\phi}_n(k_x, k_y)|^2 \, \mathrm{d}k_x \, \mathrm{d}k_y. \tag{26}$$

In practice, the averaged Green's function in wavenumber space proposed in Ref. [19] is employed to avoid the singularity of the integrand at coincidence.

As shown previously, all resonant waves have the same energy. Eqs. (23) and (26) can therefore be used to calculate the mean square velocity and radiated power when a diffuse reveberant field exists within the subsystem. Using Parseval's relation, the surface integral of Eq. (23) can be expressed in terms of the wavenumber transform, $\tilde{\phi}_n$. Combining the resulting expression with Eq. (26) then yields the average resonant

radiation efficiency

$$\sigma_{\mathrm{rad}}(\omega)=\frac{\langle\int_{-\infty}^{\infty}\int_{-\infty}^{\infty}|\tilde{\phi}_n(k_x,k_y)|^2\mathrm{Im}\{G(k_x,k_y,\omega)\}\,\mathrm{d}k_x\,\mathrm{d}k_y\rangle_{\varepsilon_x,\varepsilon_y,n/\Omega_n(\varepsilon_x,\varepsilon_y)\in\Delta\omega}}{\rho c\omega\langle\int_{-\infty}^{\infty}\int_{-\infty}^{\infty}|\tilde{\phi}_n(k_x,k_y)|^2\,\mathrm{d}k_x\,\mathrm{d}k_y\rangle_{\varepsilon_x,\varepsilon_y,n/\Omega_n(\varepsilon_x,\varepsilon_y)\in\Delta\omega}},\tag{27}$$

where strictly, $\tilde{\phi}_n$ is a function of phase constants $(\varepsilon_x,\varepsilon_y)$. In summary, the resonant radiation efficiency is obtained as a function of the wavenumber transforms of the wave fields over the wetted surface of the connection region. These wavenumber transforms are obtained from the wavenumber transforms of the wave fields over the unit cell using Eq. (22).

Some comments about the validity of Eq. (27) are given in what follows. The use of the Fourier transforms (and the Rayleigh integral) means that the current analysis is strictly only valid for flat wetted surfaces. For a curved surface, Eq. (24) is a good approximation if the curvature is not 'too small' when compared with the acoustic wavelength [22]. The surface is then effectively *unwrapped* onto a planar surface.

Below acoustic coincidence, the radiation efficiency of a homogenous flat structure is typically dominated by radiation from the edges of the structure (or, in the current analysis, from the edges of the 'connection region' to the adjacent fluid). This 'edge' radiation, in turn, depends on the boundary conditions assumed for the structure. In the previous analysis, the radiation efficiency obtained in Eq. (27) is for a connection region with Born–von Kármán (or 'periodic') boundary conditions. These boundary conditions can be viewed as being an average overall all possible boundary impedances applied to a finite panel. Small differences can be expected between this 'average' radiation efficiency and the radiation efficiency of specific boundary conditions (such as simple supported edges). It is shown in Appendix A.4 that for simple uniform flat panels, the radiation efficiency for Born–von Kármán boundary conditions is approximately half that for simply supported boundary conditions.

The current analysis is also for a baffled connection region. The effects of baffled versus unbaffled acoustic boundary conditions have been reported in Ref. [21]. Removing the baffle typically causes a reduction in radiation efficiency below coincidence (due to cancellation of the radiation from the front and back edges of the structure).

The current analysis has focused on untrimmed structures. Poroelastic noise control treatments (trim) can be included in the analysis in two ways: (i) the trim can be described explicitly by FEs and thus be part of the eigensolution in Eq. (6), the wetted surface being the outer surface of the trim or (ii) the trim can be included in the wavenumber transform of the Green's function $G(k_x,k_y,\omega)$ by using a wavenumber description of a multilayered trim [23].

4.3. Power input from random pressure loadings

This section describes the computation of the power input to a finite periodic structure loaded over a wetted surface A_N by a space and time stationary random pressure field. The blocked pressure field is defined by a space–frequency cross-spectrum $R_{pp}(\Delta X,\Delta Y,\omega)$.

The generalized force on a particular wave displacement shape $\boldsymbol{\varphi}_n(\varepsilon_x,\varepsilon_y)$ due to a blocked pressure field $p(X,Y)$ is the surface integral across the connection region of the displacement field φ_n times the pressure field. The resulting complex wave amplitude $a_n(\varepsilon_x,\varepsilon_y)$ is given by

$$a_n(\varepsilon_x,\varepsilon_y)=\frac{\int\int_{A_N}\varphi_n^*(X,Y)p(X,Y)\,\mathrm{d}X\,\mathrm{d}Y}{N_xN_y((1+\mathrm{i}\eta)\Omega_n^2(\varepsilon_x,\varepsilon_y)-\omega^2)},\tag{28}$$

where the denominator is the dynamic stiffness associated with the wave displacement shape over the larger periodic structure: the N_xN_y factor accounts for the number of cells of the structure; the terms inside the parenthesis are derived from Eq. (6) and the mass normalization adopted; the damping loss factor is function of the phase constants $(\varepsilon_x,\varepsilon_y)$ and eigensolution number n. The radiation impedance of the fluid should, ideally, also be included in the previous expression. However, the following analysis assumes light fluid loading for simplicity. The time-averaged power input into the wave is given by

$$\Pi_n(\varepsilon_x,\varepsilon_y)=\frac{1}{2}\mathrm{Re}\left\{\iint_{A_N}\mathrm{i}\omega a_n(\varepsilon_x,\varepsilon_y)\varphi_n(X,Y)p^*(X,Y)\,\mathrm{d}X\,\mathrm{d}Y\right\}.\tag{29}$$

Substituting the expression in Eq. (28) for a_n into Eq. (29), the power input is given by

$$\Pi_n(\varepsilon_x,\varepsilon_y)=\frac{1}{2N_xN_y}\mathrm{Re}\left\{\frac{\mathrm{i}\omega}{(1+\mathrm{i}\eta)\Omega_n^2(\varepsilon_x,\varepsilon_y)-\omega^2}\right.$$
$$\left.\times\iint_{A_N}\iint_{A_N}\varphi_n(X,Y)\varphi_n^*(X',Y')p^*(X,Y)p(X',Y')\,\mathrm{d}X\,\mathrm{d}Y\,\mathrm{d}X'\,\mathrm{d}Y'\right\}. \tag{30}$$

For a spatially stationary random pressure field, the time-averaged product of the pressure terms is the space–frequency cross-spectrum R_{pp}, which only depends on the distance between points along each axis ($\Delta X=X'-X$, $\Delta Y=Y'-Y$), and on frequency. The wavenumber transform of the space–frequency cross-spectrum is the wavenumber–frequency spectrum S_{pp}:

$$R_{pp}(\Delta X,\Delta Y,\omega)=\frac{1}{4\pi^2}\int_{-\infty}^{\infty}\int_{-\infty}^{\infty}S_{pp}(k_x,k_y,\omega)\mathrm{e}^{\mathrm{i}(k_x(X'-X)+k_y(Y'-Y))}\,\mathrm{d}k_x\,\mathrm{d}k_y. \tag{31}$$

Substituting Eq. (31) in Eq. (30), and inverting the order of integration gives

$$\Pi_n(\varepsilon_x,\varepsilon_y)=\frac{1}{8\pi^2N_xN_y}\mathrm{Re}\left\{\frac{\mathrm{i}\omega}{(1+\mathrm{i}\eta)\Omega_n^2(\varepsilon_x,\varepsilon_y)-\omega^2}\right\}\int_{-\infty}^{\infty}\int_{-\infty}^{\infty}|\tilde{\phi}_n(k_x,k_y)|^2S_{pp}(k_x,k_y,\omega)\,\mathrm{d}k_x\,\mathrm{d}k_y, \tag{32}$$

where it has been noted that the spectrum S_{pp} is a real valued function. $\tilde{\phi}_n$ is the wavenumber transform of the wave displacement field over the connection region, and can be obtained from the wavenumber transform of the wave field over the unit cell using Eq. (22).

For a given frequency band $\Delta\omega$, the power input into the resonant wavefield can be found by summing the contribution $\Pi_n(\varepsilon_x,\varepsilon_y)$ of all resonant waves: according to Eq. (10), the 'density' associated with each wave is $N_xN_y/4\pi^2$ so that the power input into a diffuse reverberant field is given by

$$\Pi_{\mathrm{in}}(\omega)=\frac{N_xN_y}{4\pi^2}\sum_n\left(\int_{-\pi}^{\pi}\int_{-\pi}^{\pi}\Pi_n(\varepsilon_x,\varepsilon_y)\,\mathrm{d}\varepsilon_x\,\mathrm{d}\varepsilon_y\right)_{\varepsilon_x,\varepsilon_y/\Omega_n(\varepsilon_x,\varepsilon_y)\in\Delta\omega}, \tag{33}$$

where the n summation runs over the number of phase constant surfaces. The double integral can be written as the mean value of $\Pi_n(\varepsilon_x,\varepsilon_y)$ over each phase constant surface. The expression for $\Pi_n(\varepsilon_x,\varepsilon_y)$ can be averaged over the frequency band by assuming that the spectrum S_{pp} is a relatively smooth function of frequency: the frequency-averaged value of Eq. (32) is then obtained by considering the value of the spectrum at the center frequency and by averaging the fraction term only. For resonant waves, the averaged value of the fraction tends rapidly toward $\pi/2\Delta\omega$ (independent of damping) when η tends toward zero [4] with result that

$$\Pi_{\mathrm{in}}(\omega)=\frac{1}{16\pi\Delta\omega}\sum_n\left\langle\int_{-\infty}^{\infty}\int_{-\infty}^{\infty}|\tilde{\phi}_n(k_x,k_y)|^2S_{pp}(k_x,k_y,\omega)\,\mathrm{d}k_x\,\mathrm{d}k_y\right\rangle_{\varepsilon_x,\varepsilon_y/\Omega_n(\varepsilon_x,\varepsilon_y)\in\Delta\omega}. \tag{34}$$

Similarly to the derivation of the radiation efficiency, the Born–von Kármán boundary conditions were assumed to derive Eq. (34), and the comments in the previous section regarding boundary conditions are equally applicable here. The wavenumber–frequency cross-spectrum S_{pp} associated with standard models of turbulent boundary layer and diffuse acoustic field can be found in the literature (see for example, Refs. [24,25]).

4.4. Acoustic transmission loss

In this section, the acoustic transmission loss of a periodic structure is derived, when fluids are present on both sides of the structure. Strictly, in an SEA model, the non-resonant transmission loss describes the transmission of acoustic power through the non-resonant modes of the structure (the resonant transmission path is accounted for via the resonant CLFs between the panel and adjacent fluids). In the following analysis, a diffuse acoustic field is applied on one side of the structure, and the power radiated on the other side is computed. One approach to this problem is to use the structural equation of motion, Eq. (6), with a

generalized force on the right-hand side (since a diffuse field loading can be described as a set of uncorrelated acoustic plane waves which are periodic by nature). The transmitted power can then be estimated for each angle of incidence by computing the forced response and by computing the radiated power using an expression similar to Eq. (26). However, with this approach, it is difficult to distinguish resonant and non-resonant transmissions.

The following analysis therefore adopts an alternative approach based on a recent diffuse-field reciprocity result [26]. This provides a simple expression for the (diffuse field) CLF between two acoustic cavities separated by a structure. The CLF is expressed in terms of the radiation and mechanical impedances of the structure, and can be related to the power transmission coefficient through standard formula [4, p. 485] to give

$$\tau(\omega) = \frac{16\pi}{A_N k_1^2} \sum_{rs} \mathrm{Im}\{\mathbf{D}_{\mathrm{rad}}^{(2)}\}_{rs} (\mathbf{D}_{\mathrm{tot}}^{-1} \mathrm{Im}\{\mathbf{D}_{\mathrm{rad}}^{(1)}\} \mathbf{D}_{\mathrm{tot}}^{-H})_{rs}, \tag{35}$$

where k_1 is the acoustic wavenumber in the source cavity, and A_N is the wetted surface area. The summation runs over the degrees of freedoms of the structure. $\mathbf{D}_{\mathrm{rad}}^{(i)}$ is the 'direct field' dynamic stiffness matrix that fluid i presents to the structural degrees of freedom, (i.e. the radiation stiffness obtained if the acoustic space was semi-infinite). The total dynamic stiffness $\mathbf{D}_{\mathrm{tot}}$ includes the mechanical and radiation contributions, $\mathbf{D}_{\mathrm{tot}} = \mathbf{D}_{\mathrm{str}} + \mathbf{D}_{\mathrm{rad}}^{(1)} + \mathbf{D}_{\mathrm{rad}}^{(2)}$. The calculation of the radiation stiffness of fluids 1 and 2 can be based on the same wetted face (for thin structures such as the ribbed panels shown in Fig. 2a,c,e), or two different faces (for thick structures such as double walls or extruded floors as shown in Fig. 2b,d,f).

The mechanical stiffness associated with a particular wave displacement shape $\boldsymbol{\varphi}_n(\varepsilon_x,\varepsilon_y)$ is $D_{\mathrm{str},n}(\varepsilon_x,\varepsilon_y) = N_x N_y((1+i\eta)\Omega_n^2(\varepsilon_x,\varepsilon_y) - \omega^2)$. The radiation stiffness is the surface integral of the product $\varphi_n p_n^*$ across the wetted surface of the connection region, where φ_n is the normal component of the wave displacement shape and p_n is the surface pressure induced by this displacement. The radiation stiffness can be obtained using a similar derivation to Eq. (26), and is given by

$$D_{\mathrm{rad},n}^{(i)}(\varepsilon_x,\varepsilon_y) = \frac{1}{4\pi^2} \int_{-\infty}^{\infty} \int_{-\infty}^{\infty} G_i^*(k_x,k_y,\omega) |\tilde{\phi}_n(k_x,k_y)|^2 \,\mathrm{d}k_x \,\mathrm{d}k_y. \tag{36}$$

Describing the structural field with uncorrelated waves with associated 'density' equal to $N_x N_y/4\pi^2$, Eq. (35) becomes

$$\tau(\omega) = \frac{16\pi}{A_N k_1^2} \frac{N_x N_y}{4\pi^2} \sum_n \left(\int_{-\pi}^{\pi} \int_{-\pi}^{\pi} \frac{\mathrm{Im}\{D_{\mathrm{rad},n}^{(1)}(\varepsilon_x,\varepsilon_x)\} \mathrm{Im}\{D_{\mathrm{rad},n}^{(2)}(\varepsilon_x,\varepsilon_x)\}}{|N_x N_y((1+\mathrm{i}\eta)\Omega_n^2(\varepsilon_x,\varepsilon_x) - \omega^2) + D_{\mathrm{rad},n}^{(1)}(\varepsilon_x,\varepsilon_x) + D_{\mathrm{rad},n}^{(2)}(\varepsilon_x,\varepsilon_x)|^2} \,\mathrm{d}\varepsilon_x \,\mathrm{d}\varepsilon_y \right). \tag{37}$$

The integral in Eq. (37) can be replaced by the averaged value over the phase constant space to give

$$\tau(\omega) = \frac{16\pi}{A k_1^2} \sum_n \left\langle \frac{\mathrm{Im}\{D_{\mathrm{rad},n}^{(1)}(\varepsilon_x,\varepsilon_x)\} \mathrm{Im}\{D_{\mathrm{rad},n}^{(2)}(\varepsilon_x,\varepsilon_x)\}}{|N_x N_y((1+\mathrm{i}\eta)\Omega_n^2(\varepsilon_x,\varepsilon_x) - \omega^2) + D_{\mathrm{rad},n}^{(1)}(\varepsilon_x,\varepsilon_x) + D_{\mathrm{rad},n}^{(2)}(\varepsilon_x,\varepsilon_x)|^2} \right\rangle_{\varepsilon_x,\varepsilon_y}, \tag{38}$$

where A is the area of the wetted face over a unit periodic cell. The n summation runs over the number of phase constant surfaces.

The contribution to the transmission from the waves with propagating frequency within a given frequency band $\Delta\omega$ (i.e. $\Omega_n(\varepsilon_x,\varepsilon_y) \in \Delta\omega$) defines the resonant transmission. Alternatively, the non-resonant transmission is obtained from the contribution of the waves with propagating frequency below and above the frequency band. The structural dynamic stiffness in Eq. (38) exhibits sharp frequency variations when the wave is resonant in the investigated frequency band: the resonant transmission coefficient can be analytically averaged over the frequency band by assuming that the radiation dynamic stiffness $D_{\mathrm{rad},n}^{(i)}$ are smooth function of frequency. The non-resonant transmission coefficient is a smooth function of frequency and does not require band averaging.

The previous sections have derived expressions for the modal density, engineering units data recovery, radiation efficiency, power input from pressure loading, and transmission loss of a general periodic panel. The expressions can be used to define the subsystems properties and the 'airborne' transmission paths in existing SEA models. The power input from a point force applied at a given location in a periodic structure was

derived in Ref. [18]. In order to predict structural CLFs, it is necessary to derive general expressions for the point and line impedances of periodic structures. The derivation of such methods will be discussed in a separate publication.

5. Validation examples

5.1. Honeycomb panel

Consider an aluminum composite panel made of two isotropic skins and a regular hexagonal honeycomb core. The aluminum properties are $\rho = 2700\,\mathrm{kg/m^3}$, $E = 71 \times 10^9\,\mathrm{Pa}$, $\nu = 0.3296$. The skins are 0.6 mm thick. The core is 15 mm thick, made of hexagonal cells with a foil thickness of 0.0508 mm and a side length of 5.5 mm (this corresponds to a standard honeycomb with equivalent density of $28.8\,\mathrm{kg/m^3}$). A unit cell was created of a single hexagonal structure and was meshed with 424 triangular shell elements and 232 nodes, as shown in Fig. 4. Periodic boundary conditions were enforced along the horizontal edges of both skins and along the vertical edges of the honeycomb core.

The free wavenumber analysis described in Section 3 was then performed to find the first few propagating waves in the composite. The eigensolutions of Eq. (6) were found and sorted for one direction (as the skins and core exhibit an isotropic behavior). Reference results were obtained for the flexural waves by considering the equivalent elastic material for the honeycomb core and applying Nilsson's formula [27], which is based on finding the roots of a third-order polynomial. The equivalent material properties for the core were obtained from Ref. [28]. For the in-plane waves, no significant contribution of the core is expected, and the reference results were computed according to the skin properties: $k_e = (\rho(1-\nu^2)/E)^{1/2}\omega$ and $k_s = (2\rho(1+\nu)/E)^{1/2}\omega$.

The free wavenumbers are shown as functions of frequency in Fig. 4. The reference results are the solid line, the periodic theory ones the dots. Good agreement can be observed. As explained in Ref. [27], the two parallel lines are the extensional and shear waves. The top curve corresponds to a symmetric bending wave with in-phase flexural motion of the skins. This wave exhibits a transition from the bending of the complete thickness of the composite at low frequencies where the skins undergo expansion and compression, to the bending of each skin at high frequencies. Two waves cut on at about 17 kHz. On of them is described by Nilsson's formulation and corresponds to the asymmetric 'breathing' bending wave with out-of-phase flexural motion of the skins. The other is a higher order in-plane wave with a mix of shear and extensional deformations where the skins of the panel have out-of-phase in-plane motions. It is possible to visualize the deformation associated with the computed wave by looking at the corresponding eigenvector of Eq. (6).

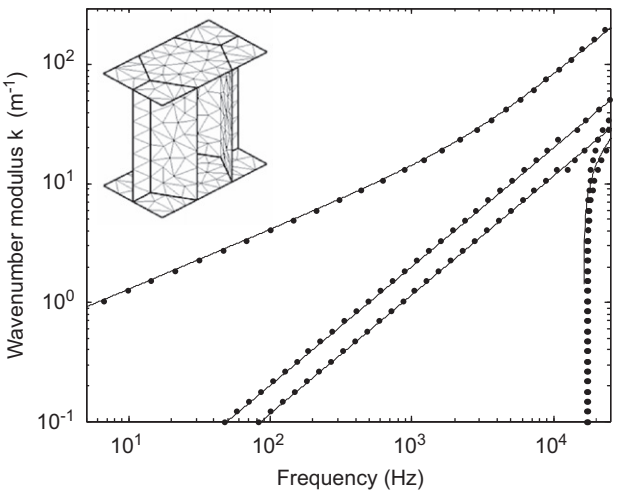

Fig. 4. Dispersion curves of the first five waves of a honeycomb sandwich panel. Dots: predictions from the current formulation; solid lines: predictions according to Ref. [27].

The modal densities of the first bending, longitudinal and shear waves were computed for a panel of 1 m^2 area, using Eqs. (11) and (13). The frequency variations of the three modal densities are shown with dots in Fig. 5. The bending modal density as given by Renji's formula [29] is plotted with a solid line, and good agreement can be observed. For the flexural wave at 10 kHz, the deformation of the periodic cell has been replicated 13×7 times with the appropriate phase lag in order to produce the picture shown in Fig. 5. A single cell has been highlighted in the middle of the structure and the propagation direction is indicated with an arrow. It can be seen that this wave motion is essentially symmetric bending of the full composite with in-phase motion of the skins.

The damping loss factor associated with the first wavetype was computed according to Eq. (15) for a particular damping distribution. The internal damping loss factor of the core is kept constant at $\eta_c = 2\%$; the damping of the skins takes the values $\eta_s = 5\%$, 3% and 1%. The predicted loss factors of the first wave are shown in Fig. 6 as functions of frequency between 50 Hz and 20 kHz. Results according to Nilsson [27] are plotted as a reference. They were obtained by substituting the undamped wavenumber (root of a third order polynomial) into the expression for the strain energy, involving complex Young's moduli, and taking the ratio of the imaginary part over the real part. The slight discrepancies observed at high frequencies are traced to the rigidity of the FE model of the cell (a finer mesh would be required as the wavelength of deformation becomes shorter; the use of triangular shell elements may also be introducing some artificial stiffness). It can be seen that the damping loss factor is not constant; as explained in Ref. [30], it actually depends on which part of the composite undergoes the most deformation (and then contributes the most to the damping mechanism). At low frequencies, the wave motion is essentially governed by the extensional motion of the skins, and the resulting loss factor is close to the skin's loss factor. At mid-frequencies near 10 kHz, the shear of the core governs the wave motion, and the damping loss factor gets close to that of the core. At high frequencies, the predominant bending of the skins makes the wave damping revert back to the skins damping value.

5.2. Ribbed structure

Consider the periodically ribbed panels described in Ref. [31]; FE meshes of the cells are shown in Figs. 8–10. The panels are made of 4 mm thick plates with ribs every 0.4 m in either one direction or two perpendicular directions. The panels dimensions are $2.7\,\text{m} \times 3.4\,\text{m}$, which approximately corresponds to 7×8 periodic cells ($0.4\,\text{m} \times 0.4\,\text{m}$). The ribs are 60 mm height, with complicated geometries and thickness between 4 and 16 mm (see Refs. [20,31] for details). All components are made of isotropic aluminum ($\rho = 2750\,\text{kg/m}^3$, $E = 71 \times 10^9\,\text{Pa}$, $\nu = 0.33$), and the base panel can be bare or treated with a damping material layer.

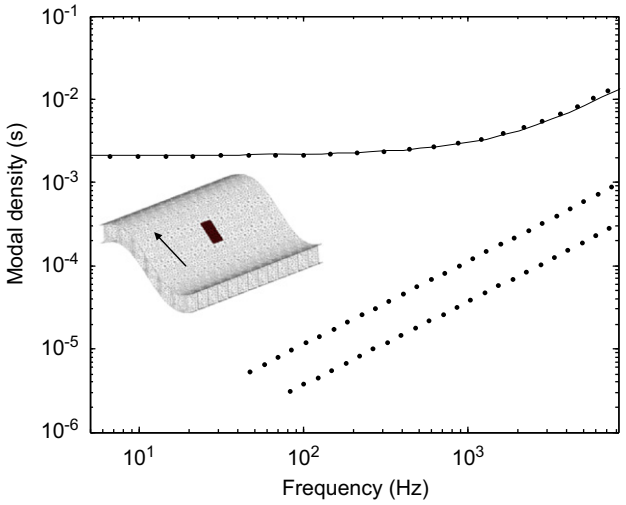

Fig. 5. Modal density associated with the extensional, shear and flexural wavetypes of a honeycomb sandwich panel of 1 m^2 area. Dots: predictions from the current formulation; solid lines: predictions according to Ref. [29].

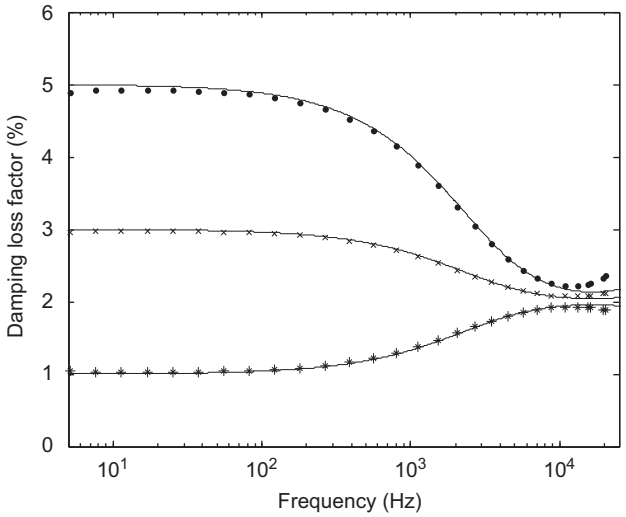

Fig. 6. Predicted loss factor of the first wave propagating in a honeycomb sandwich panel. The damping of the core is constant, $\eta_c = 2\%$. The damping of the skins is ●, $\eta_s = 5\%$; ×, $\eta_s = 3\%$; ∗, $\eta_s = 1\%$. The results according to Ref. [27] are plotted with solid lines.

The weight added by the damping treatment was estimated from Ref. [31] to be about 3.6 kg per unit area, and this was included in the models by increasing the material density to 3350 kg/m^3. The stiffness effect of the treatment was neglected, and the damping effect was included by using a higher value of structural damping loss factors: the averaged values over the investigated frequency range, $\eta = 0.6\%$ and 3% were used. The unribbed panel was also investigated with damping loss factors $\eta = 1\%$ and 5%.

The corresponding FE meshes for analysis up to 8 kHz are composed of 1288–1700 triangular shell elements and 698–918 nodes, depending on the rib configuration. For the unribbed plate, this results in approximately 3200 analysis degrees of freedom (various 'drilling' degrees of freedom are automatically removed from the analysis). The CMS reduction retained 104 normal modes and the size of the matrices in Eq. (9) were then reduced to 636. Applying the periodic boundary conditions in Eq. (5) and reducing the edge degrees of freedom resulted in 367 degrees of freedom in the matrices in Eq. (6).

The first three phase constant surfaces computed from Eq. (6) for the cross-wise stiffened panel are shown in Fig. 3. Although it cannot easily be seen in the figure, the surfaces cover the whole frequency range (at any given frequency there is at least one point in phase space), meaning that there are no stop bands for this panel in this frequency range (all waves/modes types combined). The surfaces are not symmetric about the $\varepsilon_x = \varepsilon_y$ axis because of the difference between the ribs in the x and y directions, as shown in the mesh of the cell in Fig. 10. The stiffening effect of the continuous rib in the y direction is seen to be more significant than that of the discontinuous rib in the x direction.

The modal densities of the 2.7 m × 3.4 m panels are shown in Fig. 7 for the third octave bands between 100 and 8192 Hz. The analytical result for a bare plate is plotted in gray. Good agreement is observed between this result and the prediction by Eq. (10) for the base panel. The stiffening effect of the rib can be seen at low frequencies where the modal density of the cross-wise stiffened panel is much lower than the two other ones. At higher frequencies, the modal density of the structures tends to the sum of the modal densities of each component, with the result that the modal density increases from the base panel to the simply stiffened and cross-wise stiffened ones. The peak in the band centered at 161 Hz in the modal density of the cross-wise panel is due to the cut-on of the first local mode of the cell.

The measured transmission loss of the panels with and without damping treatments are given in Refs. [20,31]. Simulations were performed using Eq. (38), where both resonant and non-resonant contributions have been included. For all three rib configurations, the treated and untreated panels have been investigated, and the effect of the damping treatment was included in the FE models of the cell as added mass and increased damping loss factor. It is worth mentioning that based on the modal density computed above, there are approximately 6500 modes in the base panel in the frequency range of interest. Comparisons

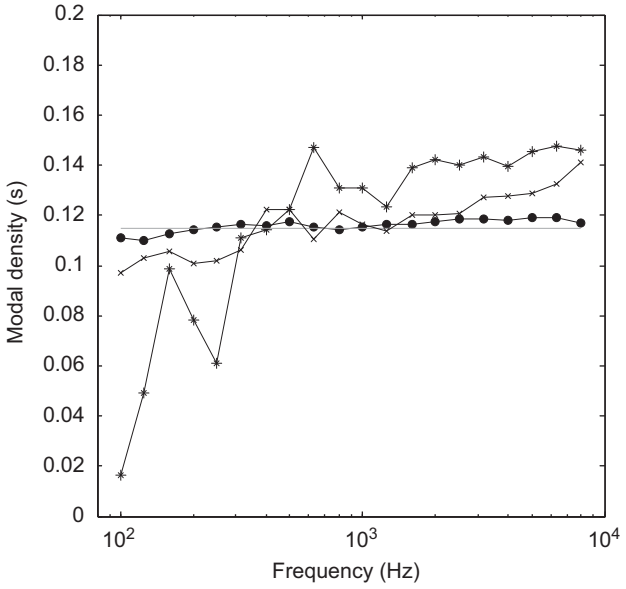

Fig. 7. Modal density of three 2.7 m × 3.4 m panels as a function of frequency. Black: predictions from the current formulation for ●, base panel; ×, simply stiffened; ∗, cross-wise stiffened; gray: analytical result for base panel.

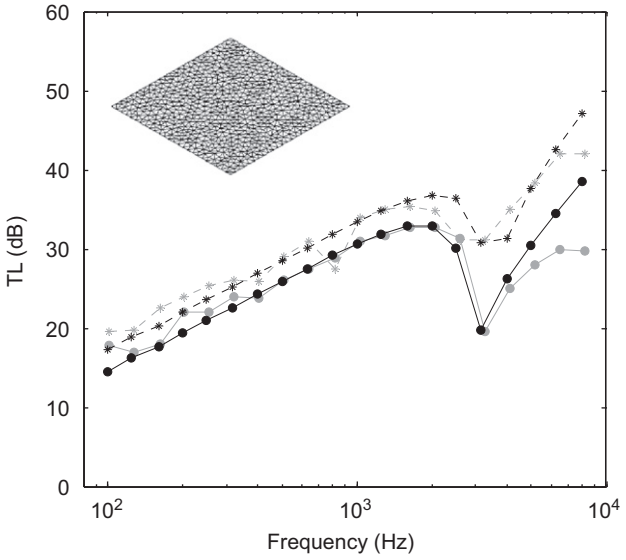

Fig. 8. Diffuse-field transmission loss of a bare panel with and without damping treatment. Black: predictions; gray: experimental data from Ref. [20,31]. ●, Untreated ($\eta = 1\%$); ∗, treated ($\eta = 5\%$ and additional mass).

between the predicted and measured data are shown in Figs. 8–10. The coincidence frequency of the unribbed panel is approximately 3000 Hz.

Overall, good agreement can be seen between the predictions and the test data (given the amount of details available regarding the structures). In all cases, the damping treatment increases the TL. For all three rib configurations, the same mass is added by the noise control treatment. It can be seen that, below coincidence, the addition of the noise control treatment has more impact on the TL for the ribbed panels than for the bare panel. This is observed on both the experimental and simulation data. The reason for this behavior is that damping only affects the resonant transmission. For the unstiffened panel, the resonant contribution is much less than the non-resonant one below the coincidence frequency; the transmission below coincidence is

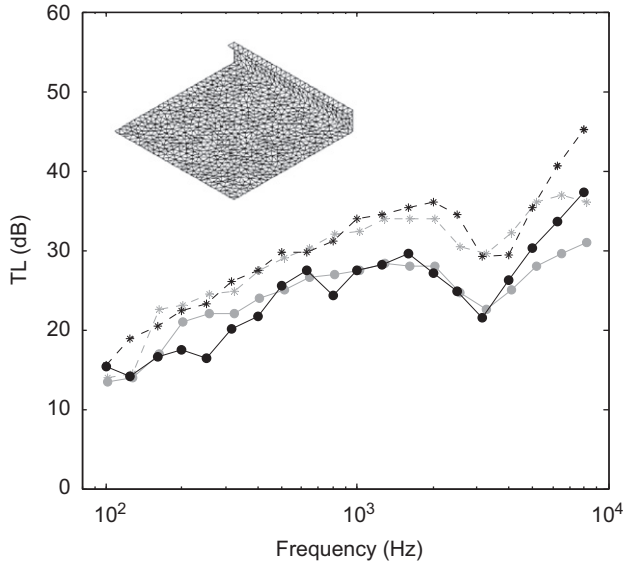

Fig. 9. Diffuse-field transmission loss of a simply stiffened panel with and without damping treatment. Black: predictions; gray: experimental data from Refs. [20,31]. ●, Untreated ($\eta = 0.6\%$); ∗, treated ($\eta = 3\%$ and additional mass).

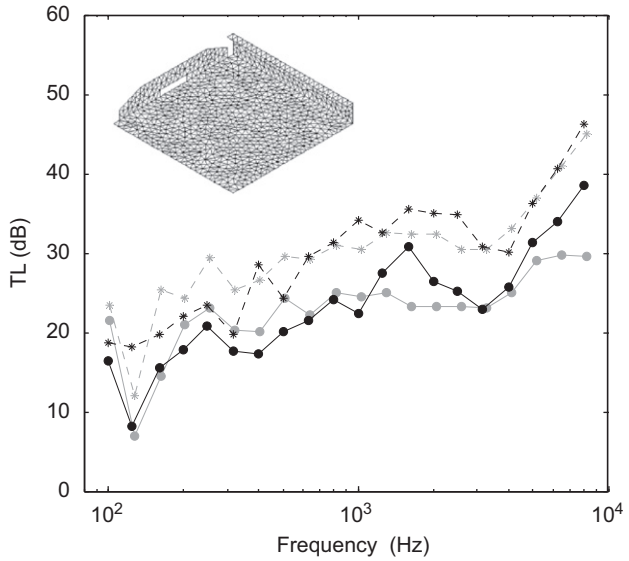

Fig. 10. Diffuse-field transmission loss of a cross-wise stiffened panel with and without damping treatment. Black: predictions; gray: experimental data from Refs. [20,31]. ●, Untreated ($\eta = 0.6\%$); ∗, treated ($\eta = 3\%$ and additional mass).

therefore fairly insensitive to damping. The increase in the TL of the bare panel below coincidence is primarily due to the mass effect of the noise control treatment. Adding stiffeners to the bare panel increases the resonant contribution to the TL. Increasing the damping therefore has a bigger influence on the TL below the coincidence frequency.

5.3. Curved structure

The effect of curvature on the modal density, sound radiation and sound transmission of a structure is now investigated for the same 4 mm thick bare aluminum panel. A damping loss factor of 5% is used in the

following analysis. The panel is curved around a single axis with a radius of curvature of $R = 2$ m; the resulting ring frequency is 432 Hz.

All simulations are performed over the third octave bands between 64 and 4096 Hz. The modal densities of the flat and curved panels made of 20×20 cells are shown in Fig. 11 as functions of frequency. The reference results from Ref. [33] are plotted in gray, while the current predictions according to Eq. (10) are plotted in black. Good agreement is observed. At the ring frequency, some discrepancies appear as the (narrowband analytical) modal density in Ref. [33] tends to infinity.

The radiation efficiencies of the flat and curved panels are shown in Fig. 12 as functions of frequency. Two predictions are provided for the flat panel: the line with circles is the computed radiation efficiency for the panel with Born–von Kármán boundary conditions (the wavenumber transform $\tilde{\phi}_n$ in Eq. (27) relates to the displacement field associated with each wave); the line with cross signs is the radiation efficiency of the panel with simply supported boundary conditions (the wavenumber transform in Eq. (27) is a linear combination of the four waves that generate a simply supported mode shape; see last paragraph of Appendix A.4). The reference result from Ref. [32] for a simply supported flat panel is plotted in gray. It can be seen that the periodic predictions with Born–von Kármán boundary conditions are approximately 3 dB lower below the coincidence frequency, while the periodic prediction with the simply supported boundary conditions show good agreement with the reference result. Both predictions yield the same values above the coincidence frequency, as the effect of the boundary conditions on the radiation properties becomes unimportant. The 3 dB difference is explained in Appendix A.4 as a direct effect of the boundary conditions.

It is interesting to note the trend of the predicted radiation efficiency of the curved structure. Below the ring frequency at 432 Hz, the stiffening effect of the curvature makes the curved panel a more efficient radiator than the flat one (a difference of approximately 15 dB can be observed). Above the ring frequency, wave propagation in the curved panel tends toward that of the flat panel as the effect of curvature diminish and this results in similar radiation efficiencies.

The radiation efficiency of the flat panel with periodic boundary conditions has been computed for three sizes of panel and is shown in Fig. 13. As a reference, the analytical formula from Ref. [32] has been plotted in gray (with a 3 dB reduction below the coincidence frequency to account for the use of simply supported boundary conditions). It can be seen that the periodic theory is able to accurately describe the variations of the radiation efficiency as a function of the panel size. This finite-size effect is accounted for by the terms N_x and N_y in Eq. (22), which relates the Fourier transforms of the displacement fields over a cell and over the entire finite structure made of $N_x \times N_y$ cells.

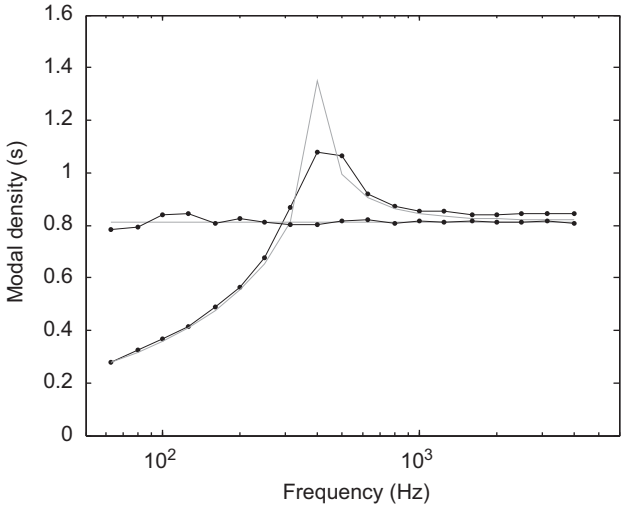

Fig. 11. Modal density of a flat and curved panels as a function of frequency. Black: predictions from the current formulation; gray: results from Refs. [33].

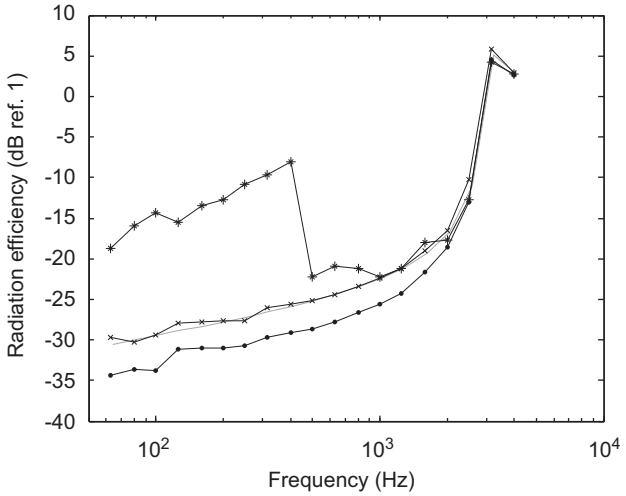

Fig. 12. Radiation efficiency of an $8\,\mathrm{m} \times 8\,\mathrm{m}$ panel as a function of frequency. Black: predictions from the current formulation; •, flat panel with Born–von Kármán boundary conditions; ×, simply supported flat panel; ∗, simply supported curved panel; gray: result for a simply supported flat panel from Ref. [32].

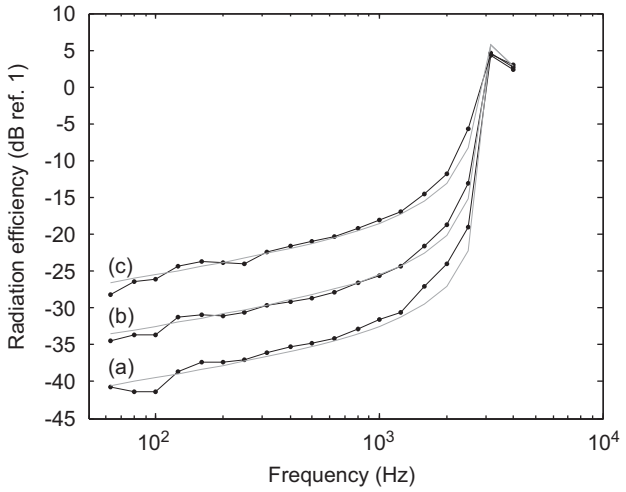

Fig. 13. Radiation efficiency of a flat panel as a function of frequency. Black: predictions from the current formulation for panel of size: (a) $40\,\mathrm{m} \times 40\,\mathrm{m}$; (b) $8\,\mathrm{m} \times 8\,\mathrm{m}$; (c) $1.6\,\mathrm{m} \times 1.6\,\mathrm{m}$; gray: results from Ref. [32] modified for boundary conditions effects.

The diffuse-field Transmission Loss of the flat and curved structures according to Eq. (38) are shown in Figs. 14 and 15 as functions of frequency. The structure was considered of infinite size by using $N = \infty$ in Eq. (22) to relate the wavenumber transforms of the displacement fields over the structure and over a single periodic cell. Reference results for the transmission through curved isotropic infinite structure can be found in Ref. [34], and are plotted with gray lines. Good agreement can be observed between the reference and periodic predictions. In particular, the different frequency regimes for transmission can be identified. For the curved structure, the transmission behavior is divided in three parts: at low frequencies the transmission is fairly flat until it drops at the ring frequency at 432 Hz; it then increases up to another drop at the coincidence frequency at 3000 Hz; it then monotonically increased with frequency. For the flat panel, only the coincidence effect is visible, so that only two frequency regimes are present.

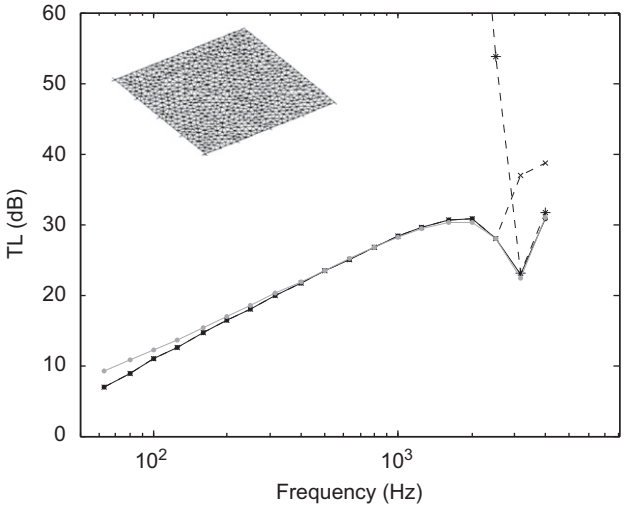

Fig. 14. Diffuse-field sound transmission loss through a flat panel. Black: predictions from the current formulation: ∗, resonant transmission; ×, non-resonant transmission; ●, total transmission. Gray: result from Ref. [34] for total transmission.

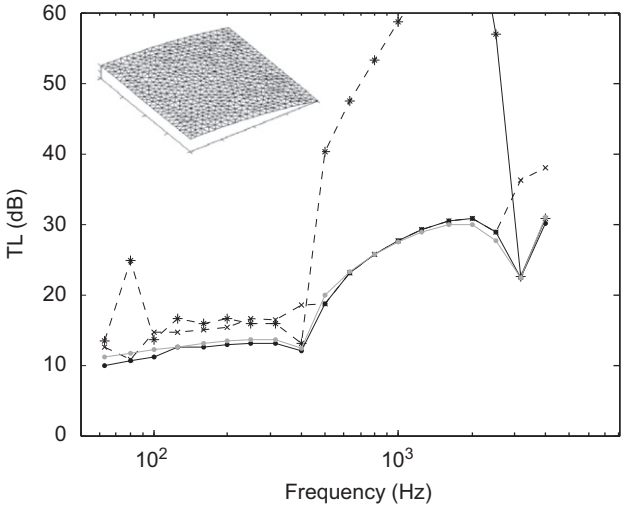

Fig. 15. Diffuse-field sound transmission loss through a curved panel. Black: predictions from the current formulation: ∗, resonant transmission; ×, non-resonant transmission; ●, total transmission. Gray: result from Ref. [34] for total transmission.

The resonant and non-resonant contributions predicted by the current formulation are plotted with dotted lines. The results are in agreement with the known behavior that transmission through flat panels is governed by non-resonant modes below the coincidence frequency and by resonant modes above. The same behavior is observed for the curved structure, with the additional frequency regime below the ring frequency where resonant and non-resonant transmissions show similar contributions.

6. Conclusions

This paper has discussed a general and efficient method for describing wave propagation in complex structural panels. A FE model was used to describe the response of a (rectangular) unit cell. CMS was then applied to the cell (in order to reduce the number of degrees of freedom), resulting in significant reductions in computational expense. Periodic boundary conditions were then applied to the edges and corners of the cell

and phase constant surfaces obtained by solving an algebraic eigenvalue problem. Expressions were derived for: modal density, section damping loss factor and 'engineering units data recovery,' using both wave and modal approaches. Additional expressions were then derived for the (resonant) radiation efficiency, input power from random pressure loads and (non-resonant) transmission loss of the panel. The latter expressions made use of an efficient Fourier transform formulation. The main contribution of the current paper is to show that the combination of CMS and periodic structure theory can be used to develop a general SEA subsystem formulation. This general SEA subsystem addresses many problems encountered with traditional analytical SEA formulations. The current paper has focused on the coupling between the structure and adjacent fluids; the extension to structural coupling (and the incorporation of pressurization and fluid loading effects) will be focus of future publications.

Acknowledgments

This work was sponsored by the Air Force Research Laboratory, Space Vehicles Directorate, Kirtland AFB, NM, USA under SBIR phase II contract F29601-02-C-0109, and by the NASA Langley Research Center, Structural Acoustics Branch, Hampton VI, USA under SBIR phase II contract NNL06AA04C. Helpful discussions with Dr. B. Gardner are gratefully acknowledged.

Appendix A. Modal approach to SEA

In this appendix, a modal approach to SEA is presented to compute the SEA properties of a periodic structure. It is shown that the eigensolutions of Eq. (6) associated with a unit periodic cell can be use to assemble the modes of a larger periodic structure with particular boundary conditions. By using a modal expansion, expressions are derived for the forced response of this larger periodic structure due to a given excitation. The expressions for the forced response are then averaged and expressions are obtained for the overall section damping loss factor, engineering unit response distribution, radiation efficiency, power input from pressure loading and transmission loss.

A.1. Waves and modes in 2D periodic structures

This section provides a brief summary of the relation between the modes of a finite 2D periodic structure with particular boundary conditions and the phase constant surfaces [18]. Consider a periodic structure with $N_x \times N_y$ cells. To simplify the analysis, a set of boundary conditions can be chosen for the edges of this larger structure that are amenable to analytical analysis. The following analysis therefore assumes Born–von Kármán (or 'periodic') boundary conditions in which the displacements of the overall structure are identical along the extreme left and right edges, and extreme top and bottom edges.

For a given phase constant surface $\Omega_n(\varepsilon_x,\varepsilon_y)$, there are N_xN_y values of the phase constants $(\varepsilon_x,\varepsilon_y)$ that satisfy the Born–von Kármán boundary conditions. These values are given by $\varepsilon_{xp} = 2\pi p/N_x$, $\varepsilon_{yq} = 2\pi q/N_y$, where p and q are integers ranging from 0 to N_x-1 and 0 to N_y-1, respectively. For a given phase constant surface, the waves with phase constants $(\varepsilon_{xp},\varepsilon_{yq})$ and $(-\varepsilon_{xp}, -\varepsilon_{yq})$ propagate at the same frequency $\omega_{pq,n} = \Omega_n(\varepsilon_{xp},\varepsilon_{yq})$. These two waves therefore combine to produce two standing waves (or 'global modes'). The displacement fields $\boldsymbol{\psi}$ of these global modes across the $\mathbf{r} = (r_x,r_y)$th cell are given by

$$\boldsymbol{\psi}_{1pq,n}(\mathbf{r}) = 2\mathrm{Re}\{\boldsymbol{\varphi}_{pq,n}\, e^{-ir_x\varepsilon_{xp}-ir_y\varepsilon_{yq}}\}, \quad \boldsymbol{\psi}_{2pq,n}(\mathbf{r}) = 2\,\mathrm{Im}\{\boldsymbol{\varphi}_{pq,n}\, e^{-ir_x\varepsilon_{xp}-ir_y\varepsilon_{yq}}\}, \tag{A.1}$$

where $\boldsymbol{\varphi}_{pq,n}$ is the wave displacement shape or eigenvector associated with the nth phase constant surface. For the global modes of Eq. (A.1) to be mass normalized, the eigenvectors of the unit cell must satisfy the condition $\boldsymbol{\varphi}^{\mathrm{H}}_{pq,n}\mathbf{M}'\boldsymbol{\varphi}_{pq,n} = 1/(2N_xN_y)$. The eigenvectors obtained from Eq. (6) using standard eigensolvers are typically mass normalized. In what follows, the normalization $\boldsymbol{\varphi}^{\mathrm{H}}_{pq,n}\mathbf{M}'\boldsymbol{\varphi}_{pq,n} = 1$ (or $\boldsymbol{\psi}^{\mathrm{H}}_{t,pq,n}\mathbf{M}'\boldsymbol{\psi}_{t,pq,n} = 2$) is therefore adopted and the $2N_xN_y$ factor is explicitly included in subsequent equations. In summary, a series of 'global modes' for a larger periodic structure can be obtained by considering the phase surfaces of a unit cell for a discrete grid of phase constants with values given by $(\varepsilon_{xp},\varepsilon_{yq})$.

A.2. Damping loss factor from a modal approach

In the following section, a modal approach is adopted by performing a discrete summation over all modes resonant within a given frequency band. A diffuse reverberant field is approximated by applying spatially incoherent 'rain-on-the-roof' excitation to the resonant modes.

Suppose that we calculate the 'resonant' damping loss factor for the mode shape associated with a given wave (i.e. the damping loss factor when the mode is excited at its resonant frequency). Since $\boldsymbol{\varphi}_{pq,n}$ is a mass-normalized eigenvector with eigenvalue $\omega_{pq,n}=\Omega_n(\varepsilon_{xp},\varepsilon_{yq})$, the denominator of Eq. (15) at frequency $\omega_{pq,n}$ is equal to $2\omega_{pq,n}^2$ so that

$$\eta_{pq,n}(\omega_{pq,n})=\frac{1}{\omega_{pq,n}^2}\sum_r \eta_r \boldsymbol{\varphi}_{pq,n}^{\mathrm{H}}(\mathbf{R}^{\mathrm{H}}\mathbf{K}_r\mathbf{R})\boldsymbol{\varphi}_{pq,n}. \tag{A.2}$$

Suppose now that we apply a force of complex magnitude $\mathbf{f}$ in the cell identified by position $\mathbf{r}=(r_x,r_y)$ within the periodic structure. The velocity response of any cell $\mathbf{r}'$ can be written in terms of the mode shapes defined in Eq. (A.1) so that

$$\mathbf{v}(\mathbf{r}')=\frac{\mathrm{i}\omega}{2N_xN_y}\sum_{t,pq,n}\frac{(\boldsymbol{\psi}_{t,pq,n}^{\mathrm{T}}(\mathbf{r})\mathbf{f})\boldsymbol{\psi}_{t,pq,n}(\mathbf{r}')}{\omega_{pq,n}^2(1+\mathrm{i}\eta_{pq,n})-\omega^2}, \tag{A.3}$$

where the summations is over all modes of the structure: the subscript t takes the values 1 and 2, p and q describe discrete values of phase constants over the region $(0<p<N_x-1,\ 0<q<N_y/2)$, and the summation n runs over all phase constant surfaces. For an isolated structure, the time-average power dissipated by the structure equals the time-average power input into the structure so that

$$P_{\mathrm{diss}}=\frac{1}{2}\mathrm{Re}\{\mathbf{f}^{\mathrm{H}}\mathbf{v}(\mathbf{r})\}=\frac{1}{2}\frac{1}{2N_xN_y}\sum_{t,pq,n}\boldsymbol{\psi}_{t,pq,n}^{\mathrm{T}}(\mathbf{r})\mathbf{f}\mathbf{f}^{\mathrm{H}}\boldsymbol{\psi}_{t,pq,n}(\mathbf{r})\mathrm{Re}\left\{\frac{\mathrm{i}\omega}{\omega_{pq,n}^2(1+\mathrm{i}\eta_{pq,n})-\omega^2}\right\}. \tag{A.4}$$

The following analysis employs a general form of 'rain-on-the-roof' excitation in which all local modes receive equal input power. This equates to '*spatially delta-correlated, broadband excitation whose magnitude at any location is proportional to the local mass density*' as discussed in Ref. [35]. The force cross-spectral matrix is thus proportional to the mass matrix, so that $\mathbf{f}\mathbf{f}^{\mathrm{H}}=\mathbf{M}'$. Due to the mass normalization of the modes, the first three terms in the summation above thus reduce to 2.

Since we are interested in the resonant damping loss factor of the section, the summation can be restricted to modes with natural frequency $\omega_{pq,n}$ within the frequency band $\Delta\omega$. The previous expression can be further simplified by averaging the input power over the frequency band to which the natural frequencies $\omega_{pq,n}$ belong. As shown by Cremer and Heckl [4, p. 329], the last term in Eq. (A.4) is closely approximated by $\pi/2\Delta\omega$, (provided the modal bandwidth is small when compared with the averaging bandwidth). This assumption is usually a good approximation in practice. The resonant band-average dissipated power is then given by

$$\langle P_{\mathrm{diss}}\rangle_{\mathbf{f},\Delta\omega}=\frac{1}{2N_xN_y}\sum_{t,pq,n}\frac{\pi}{2\Delta\omega}, \tag{A.5}$$

where the summation is over the modes with a natural frequency $\omega_{pq,n}$ within the frequency band of interest. The $\langle\ \rangle_{\mathbf{f},\Delta\omega}$ brackets indicates that the previous quantity is for rain-on-the-roof loading and is averaged over the frequency band of interest.

The time-average kinetic energy of the structure due to excitation by a force $\mathbf{f}$ can be expressed in terms of the mass matrix and the velocity response over a periodic cell. Substituting for the velocity response in Eq. (A.3) and making use of the mass orthogonality of the modes, the energy can be written as a single modal summation, so that

$$T=\frac{1}{4}N_xN_y(\mathbf{v}^{\mathrm{H}}\mathbf{M}'\mathbf{v})=\frac{1}{4}\frac{1}{4N_xN_y}\sum_{t,pq,n}\frac{\omega^2}{|\omega_{pq,n}^2(1+\mathrm{i}\eta_{pq,n})-\omega^2|^2}(2\boldsymbol{\psi}_{t,pq,n}^{\mathrm{T}}\mathbf{f}\mathbf{f}^{\mathrm{H}}\boldsymbol{\psi}_{t,pq,n}). \tag{A.6}$$

Using the cross-spectral matrix for the rain-on-the-roof excitation, the term inside the bracket reduces to 4. Considering only the resonant energy (i.e. $\omega_{pq,n} \in \Delta\omega$), and averaging over the frequency band $\Delta\omega$ gives

$$\langle T \rangle_{\mathbf{f},\Delta\omega} = \frac{1}{4N_x N_y} \sum_{t,pq,n} \frac{\pi}{2\omega_{pq,n}\eta_{pq,n}\Delta\omega}. \tag{A.7}$$

The damping loss factor associated with the average response of the structure in a band centered at the frequency ω is the ratio of the average power dissipated over twice the average kinetic energy time the circular frequency,

$$\eta_s(\omega) = \frac{\langle P_{\mathrm{diss}} \rangle_{\mathbf{f},\Delta\omega}}{2\omega \langle T \rangle_{\mathbf{f},\Delta\omega}} = \left(\left\langle \frac{1}{\eta_{pq,n}} \right\rangle_{pq,n/\omega_{pq,n} \in \Delta\omega} \right)^{-1}, \tag{A.8}$$

where use has been made of the fact that $\omega_{pq,n}$ is close to the center band frequency (since only the resonant modes are included in the expressions of the power dissipated and the kinetic energy).

Under the condition that the structure has a high modal overlap, the terms in Eq. (A.8) are smooth functions of p and q, and the average over the discrete values of p and q can be replaced by an average over the continuous values of phase constant surfaces [18]. Alternatively, if the ensemble average of the quantities is considered, then the frequency sums can be averaged across the ensemble of random structures where the modes are random quantities [1]. The ensemble mean is given by a similar continuous average where the modal density is introduced rather than $\Delta\omega$. This relaxes the requirement for high modal overlap and frequency averaging. The reason why both averaging approaches yield the same result is that a single system with high modal overlap has a response that is similar to the ensemble average (according to the SEA variance theory [1] which shows that the ensemble variance is inversely proportional to the modal overlap). The ensemble average damping is therefore written as follows:

$$\eta_s(\omega) = (\langle 1/\eta_n(\varepsilon_x, \varepsilon_y) \rangle_{\varepsilon_x,\varepsilon_y,n/\Omega_n(\varepsilon_x,\varepsilon_y) \in \Delta\omega})^{-1}. \tag{A.9}$$

This result differs from Eq. (17), where the average damping obtained using a wave approach was shown to be the averaged value of the wave damping loss factors over the phase space. This is related to the assumptions introduced in the modal derivation. In particular, the rain-in-the-roof loading injects equal power into each mode. For a loading yielding equal energy of each mode, the modal derivation would yield to Eq. (17).

A.3. Engineering units data recovery from a modal approach

Eq. (A.3) gives the velocity response of the periodic structure to a force $\mathbf{f}$ applied in the cell with position $\mathbf{r}'$. Following a similar modal approach to the previous section, the cross-spectral velocity matrix in a cell $\mathbf{r}$ is obtained for rain-on-the-roof loading, and by using the mass orthogonality of the mode shapes the double modal summation is reduced to a single summation. Grouping the 1,pq and 2,pq modal contributions then gives the following expression for the cross-spectral velocity matrix

$$\langle \mathbf{v}(\mathbf{r})\mathbf{v}^{\mathrm{H}}(\mathbf{r}) \rangle_{\mathbf{f}} = \frac{1}{(2N_x N_y)^2} \sum_{pq,n} \frac{\omega^2}{|\omega_{pq,n}^2(1 + \mathrm{i}\eta_{pq,n}) - \omega^2|^2} 2(\boldsymbol{\psi}_{1,pq,n}(\mathbf{r})\boldsymbol{\psi}_{1,pq,n}^{\mathrm{T}}(\mathbf{r}) + \boldsymbol{\psi}_{2,pq,n}(\mathbf{r})\boldsymbol{\psi}_{2,pq,n}^{\mathrm{T}}(\mathbf{r})). \tag{A.10}$$

In Ref. [18], it was shown that the term in parentheses equals $4\mathrm{Re}\{\boldsymbol{\varphi}_{pq,n}\boldsymbol{\varphi}^{\mathrm{H}}{}_{pq,n}\}$, where $\boldsymbol{\varphi}_{pq,n}$ is the wave displacement shape from Eq. (A.1). Since interest lies in recovering the engineering units response associated with a diffuse reverberant field, only the contribution of the resonant modes is considered in Eq. (A.10). The summations over pq,n are consequently restricted to the modes with natural frequency within the frequency band of interest $\Delta\omega$. To average Eq. (A.10) over the band, the fraction in the summation is approximated by $\pi/(2\eta_{pq,n}\omega_{pq,n}\Delta\omega)$ [4]. This result is valid if there are several modes in the band and if the damping is not too great (the modal bandwidth must be small when compared with the averaging bandwidth).

Eq. (A.10) then becomes

$$\langle \mathbf{v}(\mathbf{r})\mathbf{v}^{\mathrm{H}}(\mathbf{r})\rangle_{\mathbf{f},\Delta\omega} = \frac{8}{(2N_xN_y)^2}\sum_{pq,n}\frac{\pi}{2\eta_{pq,n}\omega_{pq,n}\Delta\omega}\mathrm{Re}\{\boldsymbol{\varphi}_{pq,n}\boldsymbol{\varphi}_{pq,n}^{\mathrm{H}}\}. \tag{A.11}$$

The total resonant energy averaged over the frequency band is given as two times the expression in Eq. (A.7) so that the cross-spectral velocity matrix of the periodic structure is given in term of the total energy E by

$$\mathbf{S}_{vv} = \frac{2E}{N_xN_y}\frac{\sum_{pq,n}1/\omega_{pq,n}\eta_{pq,n}\mathrm{Re}\{\boldsymbol{\varphi}_{pq,n}\boldsymbol{\varphi}_{pq,n}^{H}\}}{\sum_{pq,n}1/\omega_{pq,n}\eta_{pq,n}} \sim \frac{2E}{N_xN_y}\langle \mathrm{Re}[\boldsymbol{\varphi}_{pq,n}\boldsymbol{\varphi}_{pq,n}^{H}]\rangle_{pq,n/\omega_{pq,n}\in\Delta\omega}, \tag{A.12}$$

where the damping loss factor $\eta_{pq,n}$ is given in Eq. (A.2). The last expression of Eq. (A.12) was obtained by assuming that the resonant waves propagating frequencies and damping loss factors are uniform across the frequency band. Similarly to the damping loss factor, the average over the discrete values of p and q is replaced by an average over the continuous values of phase constant surfaces (invoking ensemble statistics) to give

$$\mathbf{S}_{vv} = \frac{2E}{N_xN_y}\langle \mathrm{Re}\{\boldsymbol{\varphi}_n\boldsymbol{\varphi}_n^{\mathrm{H}}\}\rangle_{\varepsilon_x,\varepsilon_y,n/\Omega_n(\varepsilon_x,\varepsilon_y)\in\Delta\omega}. \tag{A.13}$$

This result differs from Eq. (18) obtained with a wave approach in that the modal result is the real part of the wave result. This is due to the assumptions introduced in the modal derivation: the modes each exhibit in-phase motion and they are incoherently excited by the rain-on-the-roof loading, therefore producing a real cross-spectrum. Both results are identical for the modulus square velocity obtained from the diagonal entries of the cross-spectral velocity matrix.

A.4. Radiation efficiency from a modal approach

In this section, a modal approach is adopted to compute the average radiation efficiency of a periodic structure coupled to a fluid across a finite rectangular 'connection region' of dimension $N_x \times N_y$ cells. Similarly to the wave approach presented in the main text, the normal component of the mode shape displacement field $\boldsymbol{\psi}$ defined in Eq. (A.1) is obtained over the wetted surface of the unit cell. The resulting displacement is represented by the scalar field $\psi(x,y)$. In this section, and the two following sections about acoustic coupling, the (resonant) structural damping loss factor is assumed to be constant within each frequency band of interest (in practice, the averaged value found from Eqs. (17) or (A.8) is used).

The average mean square velocity and the radiated power are expressed in terms of the *in-vacuo* resonant modes of the structure. Eq. (A.3) gives the velocity response of the periodic structure to a force of magnitude $\mathbf{f}$ applied in the $\mathbf{r}$th cell. This can be written in terms of the displacement field projected onto the wetted face of the connection region as

$$v(X,Y) = \frac{\mathrm{i}\omega}{2N_xN_y}\sum_{t,pq,n}\frac{f\psi_{t,pq,n}(X_0,Y_0)\psi_{t,pq,n}(X,Y)}{\omega_{pq,n}^2(1+i\eta)-\omega^2}, \tag{A.14}$$

where f is the complex magnitude of the point force applied at (X_0,Y_0) in the direction normal to the face. The mean squared velocity can be found by integrating $|v(X,Y)|^2/2A_N$ across the wetted surface. The expression can then be averaged over the rain-on-the-roof loading (uncorrelated forces with magnitude $|f|^2=\rho(X_0,Y_0)$) to yield a double integral over the wetted surface. The double summation collapses to a single summation because of the mass orthogonality of the mode shapes. Grouping the pq contributions together then gives the following expression for the average mean square velocity

$$\langle\overline{v^2}\rangle_f = \frac{1}{4A_NN_xN_y}\sum_{pq,n}\frac{\omega^2}{|\omega_{pq,n}^2(1+\mathrm{i}\eta)-\omega^2|^2}\iint_{A_N}(\psi_{1pq,n}^2(X,Y)+\psi_{2pq,n}^2(X,Y))\,\mathrm{d}X\,\mathrm{d}Y, \tag{A.15}$$

where p,q represent points in phase space ($0<p<N_x-1$, $0<q<N_y/2$). The previous summation can be restricted to resonant modes (since interest lies in the radiation efficiency of the resonant modes of the structure). The term in the integral was shown in Ref. [18] to be equal to $4|\varphi_{pq,n}(X,Y)|^2$, where $\varphi_{pq,n}$ is the

projection of the wave displacement shape. Using Parseval's relation, the surface integral can be expressed in terms of the wavenumber transform $\tilde{\phi}_{pq,n}$ of the displacement field over the wetted surface of the connection region A_N so that

$$\langle\overline{v^2}\rangle_f = \frac{1}{4\pi^2}\frac{1}{A_N N_x N_y}\sum_{pq,n}\frac{\omega^2}{|\omega_{pq,n}^2(1+\mathrm{i}\eta)-\omega^2|^2}\int_{-\infty}^{\infty}\int_{-\infty}^{\infty}|\tilde{\phi}_{pq,n}(k_x,k_y)|^2\,\mathrm{d}k_x\,\mathrm{d}k_y. \tag{A.16}$$

The wavenumber transform $\tilde{\phi}_{pq,n}$ of the projected wave shape over the connection region is obtained from the wavenumber transform over the unit cell using Eq. (22). Averaging over a frequency band $\Delta\omega$ centered at ω gives

$$\langle\overline{v^2}\rangle_{f,\Delta\omega} = \frac{1}{4\pi^2}\frac{1}{A_N N_x N_y}\frac{\pi}{2\eta\omega\Delta\omega}\sum_{pq,n}\int_{-\infty}^{\infty}\int_{-\infty}^{\infty}|\tilde{\phi}_{pq,n}(k_x,k_y)|^2\,\mathrm{d}k_x\,\mathrm{d}k_y. \tag{A.17}$$

Consider now the problem of predicting the acoustic power radiated by the resonant modes of the structure. The time-average power radiated by the velocity field $v(X,Y)$ is given by the surface integral of the product $1/2\,\mathrm{Re}\{vp^*\}$, where p is the surface pressure induced by the velocity field. Substituting Eq. (A.14) for the velocity field gives the following expression for the radiated power:

$$\Pi = \frac{1}{2}\mathrm{Re}\left\{\sum_{t,pq,n}\frac{\mathrm{i}\omega f\psi_{t,pq,n}(X_0,Y_0)}{2N_xN_y(\omega_{pq,n}^2(1+\mathrm{i}\eta)-\omega^2)}\iint_{A_N}\psi_{t,pq,n}(X,Y)p^*(X,Y)\,\mathrm{d}X\,\mathrm{d}Y\right\}. \tag{A.18}$$

The radiated pressure that arises when the structure is excited by a single point force can be written in terms of the following modal expansion:

$$p(X,Y) = \frac{1}{2N_xN_y}\sum_{t,pq,n}\frac{f_0\psi_{t,pq,n}(X_0,Y_0)p_{t,pq,n}(X,Y)}{\omega_{pq,n}^2(1+\mathrm{i}\eta)-\omega^2}, \tag{A.19}$$

where $p_{t,pq,n}$ is the pressure field due to the vibration field corresponding to the modal normal displacement shape $\psi_{t,pq,n}$. Substituting Eq. (A.19) into Eq. (A.18), and averaging the radiated power over all rain-on-the-roof loading locations, gives

$$\langle\Pi\rangle_f = \frac{1}{2}\frac{1}{2N_xN_y}\mathrm{Re}\left\{\sum_{t,pq,n}\frac{\mathrm{i}\omega}{|\omega_{pq,n}^2(1+\mathrm{i}\eta)-\omega^2|^2}\iint_{A_N}\psi_{t,pq,n}(X,Y)p_{t,pq,n}^*(X,Y)\,\mathrm{d}X\,\mathrm{d}Y\right\}. \tag{A.20}$$

If the wetted surface is planar then the pressure radiated by the mode shape $\psi_{t,pq,n}$ can be written using Rayleigh's integral and the free-field Green's function: the pressure $p_{t,pq,n}$ is then found from Eq. (24) where $\psi_{t,pq,n}$ is substituted to φ_n. Inserting the resulting integral over space into Eq. (A.20) gives an expression for the radiated power in terms of a double surface integral. The Green's function can be expressed in term of its wavenumber transform, $G(k_x,k_y,\omega)=\mathrm{i}\rho\omega^2/(k^2-k_x^2-k_y^2)^{1/2}$ [19]. By inverting the order of the wavenumber and spatial integrals, Eq. (A.20) can be rewritten

$$\langle\Pi\rangle_f = \frac{1}{2}\frac{1}{2N_xN_y}\mathrm{Re}\left\{\sum_{pq,n}\frac{\mathrm{i}\omega}{\left|\omega_{pq,n}^2(1+\mathrm{i}\eta)-\omega^2\right|^2}\frac{1}{4\pi^2}\int_{-\infty}^{\infty}\int_{-\infty}^{\infty}G^*(k_x,k_y,\omega)J_{pq,n}(k_x,k_y)\,\mathrm{d}k_x\,\mathrm{d}k_y\right\}, \tag{A.21}$$

where

$$J_{pq,n} = \iint_{A_N}\iint_{A'_N}[\psi_{1pq,n}(X,Y)\psi_{1pq,n}^*(X',Y')+\psi_{2pq,n}(X,Y)\psi_{2pq,n}^*(X',Y')] \times \mathrm{e}^{\mathrm{i}(k_x(X'-X)+\mathrm{i}k_y(Y'-Y))}\,\mathrm{d}X\,\mathrm{d}Y\,\mathrm{d}X'\,\mathrm{d}Y'.$$

The term in the brackets in the expression for $J_{pq,n}$, was shown in Ref. [18] to be equal to $2\varphi_{pq,n}(x,y)\varphi_{pq,n}^*(x',y')\mathrm{e}^{-\mathrm{i}\beta}+2\varphi_{pq,n}^*(x,y)\varphi_{pq,n}(x',y')\mathrm{e}^{\mathrm{i}\beta}$, where $\beta=r_x\varepsilon_{xp}+r_y\varepsilon_{yq}$, and $\varphi_{pq,n}$ is the projected wave

shape across the unit cell, r_x and r_y are the coordinate of the cell where the integration is performed. ε_{xp} and ε_{yq} are the phase constant associated with the pq,n mode. The $J_{pq,n}$ integrals over the connection region can be split in N_xN_y integrals over the local cells, and the integration variables changed from global to local to give

$$J_{pq,n}(k_x,k_y) = 2|\tilde{\phi}_{pq,n}(k_x,k_y)|^2 + 2|\tilde{\phi}_{pq,n}(-k_x,-k_y)|^2, \tag{A.22}$$

where $\tilde{\phi}_{pq,n}$ is the wavenumber transform of a given wave shape over the connection region. This can be obtained from the wavenumber transform of the wave shape over the unit cell using Eq. (22). The function G is a symmetric function of k_x and k_y. The two terms in $J_{pq,n}$ therefore contribute equally to the integral in Eq. (A.21).

The radiated power can be averaged over the resonant modes in the frequency band of interest. The fraction exhibits some resonances and anti-resonances, while the integral is expected to be a smoother function of frequency. The frequency average is therefore performed by considering the value at the center band ω for the integral, and replacing the fraction by $i\pi/(2\eta\omega^2\Delta\omega)$. Eqs. (A.21) and (A.22) can then be combined to give

$$\langle \Pi \rangle_{f,\Delta\omega} = \frac{1}{4\pi^2}\frac{1}{N_xN_y}\frac{\pi}{2\eta\omega^2\Delta\omega}\sum_{pq,n}\int_{-\infty}^{\infty}\int_{-\infty}^{\infty}|\tilde{\phi}_{pq,n}(k_x,k_y)|^2 \mathrm{Im}\{G(k_x,k_y,\omega)\}\mathrm{d}k_x\,\mathrm{d}k_y. \tag{A.23}$$

Combining Eqs. (A.17) and (A.23) then yields the averaged radiation efficiency of the resonant modes in the band centered at ω:

$$\sigma_{\mathrm{rad}}(\omega) = \frac{\langle \Pi \rangle_{f,\Delta\omega}}{\rho c A_N \langle \overline{v^2} \rangle_{f,\Delta\omega}} = \frac{\sum_{pq,n}\int_{-\infty}^{\infty}\int_{-\infty}^{\infty}|\tilde{\phi}_{pq,n}(k_x,k_y)|^2 \mathrm{Im}\{G(k_x,k_y,\omega)\}\mathrm{d}k_x\,\mathrm{d}k_y}{\rho c\omega\sum_{pq,n}\int_{-\infty}^{\infty}\int_{-\infty}^{\infty}|\tilde{\phi}_{pq,n}(k_x,k_y)|^2\mathrm{d}k_x\,\mathrm{d}k_y}, \tag{A.24}$$

where only the resonant modes are included in the pq,n summations. The summation over the resonant normal modes in Eq. (A.24) can be replaced by integrating the phase constant surfaces over the resonant region of phase space $\Omega_n(\varepsilon_x,\varepsilon_y)\in\Delta\omega$: this yields to Eq. (27) which was derived from a wave approach.

In the special case of an orthotropic structure, the four waves with phase constant pairs $(\pm\varepsilon_x,\ \pm\varepsilon_y)$ propagate at the same frequency. By using the values $\varepsilon_{xp} = p\pi/N_x$ and $\varepsilon_{yq} = q\pi/N_y$, with p and q integers ranging from 0 to N_x-1 and N_y-1, the combination of the displacement fields associated with the four waves yields a stationary simply supported mode shape whose wavenumber transform on the whole structure is given by $\tilde{\phi}_{\varepsilon_x,\varepsilon_y}(k_x,k_y) + \tilde{\phi}^*_{\varepsilon_x,\varepsilon_y}(-k_x,-k_y) - \tilde{\phi}_{\varepsilon_x,-\varepsilon_y}(k_x,k_y) - \tilde{\phi}^*_{\varepsilon_x,-\varepsilon_y}(-k_x,-k_y)$. Using the combination of these four terms in Eq. (A.24) yields the averaged radiation efficiency of the simply supported periodic structure. When the structure is not orthotropic, or if the boundary conditions are not known, the radiation efficiency with the Born–von Kármán boundary conditions can be used. It is seen from Eq. (A.24) to be equivalent to an average over the free waves propagating in the structure, and therefore corresponds to the radiation of a plate with anechoic boundary condition (no wave reflection at the edges). It is known that the boundary conditions of a flat plate have a significant impact on radiation below the coincidence frequency, due to the coherence effects between the incident and reflected waves at the edges. In Eq. (62) of Ref. [4, p. 529], the power radiated below coincidence by a semi-infinite plate with a wave normally incident and reflected at the edge is shown to be proportional to $(1+r^2-2r\cos\gamma)$, where $re^{i\gamma}$ is the wave complex reflection coefficient. The modulus squared velocity is proportional to $(1+r^2+2r\cos(\gamma-2k_bx))$, with x the distance from the edge and k_b the bending wavenumber, and the resulting space average velocity is proportional to $(1+r^2)$. The ratio of power radiated over mean square velocity is thus proportional to 1 for the anechoic boundary ($r=0$), and 2 for the simply supported one ($re^{i\gamma}=-1$). From this simple analysis, one expects the radiation efficiency of a flat plate with Born–von Kármán boundary conditions to be half the value of the plate with simply supported boundary conditions. The effects of the boundary conditions are significant below the coincidence frequency for homogenous structures because the radiation is then dominated by edge and corner effects. For ribbed structures, when the structural wavelength is of similar size or shorter than the ribs spacing, these edge effects become less important.

A.5. Power input from random pressure loadings from a modal approach

This section describes the computation of the power input to the resonant modes of a finite periodic structure loaded by a space and time stationary random pressure field over a connection region with wetted surface A_N. The blocked pressure field is defined by a space–frequency cross-spectrum function $R_{pp}(\Delta X, \Delta Y, \omega)$. The projection of each mode shape across the wetted surface is given by $\psi_{t,pq,n}$. The modal response $a_{t,pq,n}$ due to the pressure loading is given by:

$$(2N_xN_y)(\omega_{pq,n}^2(1+\mathrm{i}\eta)-\omega^2)a_{t,pq,n}(\omega)=\iint_{A_N}\psi_{t,pq,n}^*(X,Y)p(X,Y)\,\mathrm{d}X\,\mathrm{d}Y, \tag{A.25}$$

where the right-hand-side term is the generalized modal force due to the blocked pressure field. The radiation impedance of the fluid should, ideally, also be included in the previous expression. However, the following analysis assumes light fluid loading for simplicity. The total time-averaged power input is the sum of each modal contribution:

$$\Pi_{in}(\omega)=\frac{1}{2}\sum_{t,pq,n}\mathrm{Re}\left\{\iint_{A_N}\mathrm{i}\omega a_{t,pq,n}(\omega)\psi_{t,pq,n}(X,Y)p^*(X,Y,\omega)\,\mathrm{d}X\,\mathrm{d}Y\right\}. \tag{A.26}$$

Substituting Eq. (A.25) in Eq. (A.26) and regrouping the pairs of pq,n modes yields

$$\begin{aligned}\Pi_{\mathrm{in}}(\omega)=\frac{1}{4N_xN_y}\sum_{pq,n}\mathrm{Re}\Bigg\{&\frac{\mathrm{i}\omega}{\omega_{pq,n}^2(1+\mathrm{i}\eta)-\omega^2}\\&\times\iint_{A_N}\iint_{A'_N}[\psi_{1pq,n}(X,Y)\psi_{1pq,n}^*(X',Y')+\psi_{2pq,n}(X,Y)\psi_{2pq,n}^*(X',Y')]\\&\times p^*(X,Y,\omega)p(X',Y',\omega)\,\mathrm{d}X\,\mathrm{d}Y\,\mathrm{d}X'\,\mathrm{d}Y'\Bigg\},\end{aligned} \tag{A.27}$$

where the summation runs over the phase plane ($0<p<N_x-1$, $0<q<N_y/2$). For a spatially stationary random pressure field, the time-averaged product of the pressure terms is the cross-correlation function R_{pp}, and it can be expressed in terms of the wavenumber–frequency cross-spectrum using Eq. (31). Substituting Eq. (31) in Eq. (A.27), and inverting the order of integration gives

$$\Pi_{\mathrm{in}}(\omega)=\frac{1}{16\pi^2N_xN_y}\sum_{pq,n}\mathrm{Re}\left\{\frac{\mathrm{i}\omega}{\omega_{pq,n}^2(1+\mathrm{i}\eta)-\omega^2}\int_{-\infty}^{\infty}\int_{-\infty}^{\infty}S_{pp}(k_x,k_y,\omega)J_{pq,n}(k_x,k_y)\,\mathrm{d}k_x\,\mathrm{d}k_y\right\}, \tag{A.28}$$

where J_{pq} was defined in Eq. (A.21). Substituting into Eq. (A.28) the expression in Eq. (A.22) gives

$$\Pi_{\mathrm{in}}(\omega)=\frac{1}{4\pi^2N_xN_y}\sum_{pq,n}\mathrm{Re}\left\{\frac{\mathrm{i}\omega}{\omega_{pq,n}^2(1+\mathrm{i}\eta)-\omega^2}\right\}\int_{-\infty}^{\infty}\int_{-\infty}^{\infty}S_{pp}(k_x,k_y,\omega)|\tilde{\phi}_{pq,n}(k_x,k_y)|^2\,\mathrm{d}k_x\,\mathrm{d}k_y, \tag{A.29}$$

where it has been noted that S_{pp} is a real valued function. $\tilde{\phi}_{pq,n}$ is the wavenumber transform of the wave shape over the connection region, and it can be obtained from the wavenumber transform of the wave shape over the unit cell using Eq. (22).

The power input into the resonant modes of the structure can be found by keeping in the pq,n summation only the modes with natural frequency within the frequency band of interest. Assuming that the spectrum S_{pp} is relatively smooth across the frequency band of interest, the frequency-averaged value of Eq. (A.29) can be obtained by considering the value of the cross-spectrum at the center frequency and by averaging the fraction term only (as in previous sections). For the resonant modes, the averaged value of the fraction tends rapidly toward $\pi/2\Delta\omega$ when η tends toward zero [4].

The summation over the resonant modes can be replaced by a continuous sum over the phase constant surfaces (each containing $N_xN_y/2$ pq pairs), so that Eq. (A.29) becomes

$$\langle \Pi_{in}(\omega)\rangle_{\Delta\omega} = \frac{1}{16\pi\Delta\omega}\sum_n \left\langle \int_{-\infty}^{\infty}\int_{-\infty}^{\infty} S_{pp}(k_x,k_y,\omega)|\tilde{\phi}_n(k_x,k_y)|^2\,\mathrm{d}k_x\,\mathrm{d}k_y \right\rangle_{\varepsilon_x,\varepsilon_y/\Omega_n(\varepsilon_x,\varepsilon_y)\in\Delta\omega}, \tag{A.30}$$

where strictly, $\tilde{\phi}_n$ is a function of phase constants $(\varepsilon_x,\varepsilon_y)$. The n summation runs over the number of phase constant surfaces. This result is identical to Eq. (34), which was derived from a wave approach.

A.6. Transmission loss from a modal approach

A modal description of the structure response is used to derive the transmission loss from Eq. (35). If the modes of the periodic structure are used as degrees of freedom, the mechanical stiffness matrix is diagonal with entries $(\boldsymbol{D}_{\mathrm{str}})_{t,pq,n} = 2N_xN_y(\omega_{pq,n}^2(1+i\eta)-\omega^2)$. If the fluid loading is light, it can be assumed that the fluid does not couple the modes and the matrix $\mathbf{D}_{\mathrm{tot}}$ is therefore diagonal, with the result that a single summation remains in Eq. (35):

$$\tau(\omega) = \frac{16\pi}{A_N k_1^2}\sum_{pq,n}\frac{\mathrm{Im}\{D^{(2)}_{\mathrm{rad},pq,n}\}\mathrm{Im}\{D^{(1)}_{\mathrm{rad},pq,n}\}}{|2N_xN_y(\omega_{pq,n}^2(1+\mathrm{i}\eta)-\omega^2)+D^{(1)}_{\mathrm{rad},pq,n}+D^{(2)}_{\mathrm{rad},pq,n}|^2}, \tag{A.31}$$

where the contributions of modes $\psi_{1pq,n}$ and $\psi_{2pq,n}$ have been combined. Grouping the pq,n contributions at this stage is not strictly valid as some cross products terms will artificially appear in the numerator of Eq. (A.31). Since the imaginary part of the radiation stiffness is necessarily positive, the maximum error introduced by the grouping is a factor of two. The summation over pq,n covers all the modes of the structure: p and q describe points in phase space ($0<p<N_x-1$, $0<q<N_y/2$) and n runs over the number of phase constant surfaces.

The self-radiation dynamic stiffness of each pair of modes is defined as

$$D^{(i)}_{\mathrm{rad},pq,n}(\omega) = \iint_{A_N}[\psi^*_{1pq,n}(X,Y)p_{1pq,n}(X,Y)+\psi^*_{2pq,n}(X,Y)p_{2pq,n}(X,Y)]\,\mathrm{d}X\,\mathrm{d}Y, \tag{A.32}$$

where $p_{t,pq,n}$ is the pressure radiated by the modal vibration field $\psi_{t,pq,n}$. This surface integral is the sum of two terms given by Eq. (A.20), and following a similar derivation it can be written as follows:

$$D^{(i)}_{\mathrm{rad},pq,n}(\omega) = \frac{1}{\pi^2}\int_{-\infty}^{\infty}\int_{-\infty}^{\infty}|\tilde{\phi}_{pq,n}(k_x,k_y)|^2 G_i^*(k_x,k_y,\omega)\,\mathrm{d}k_x\,\mathrm{d}k_y, \tag{A.33}$$

where G_i is the wavenumber transform of the free-field Green function of a baffled structure in the fluid i, and $\tilde{\phi}_{pq,n}$ is the wavenumber transform of the wave shape across the connection region. The wavenumber transform is obtained from the wavenumber transform of the wave shape over the unit cell via Eq. (22).

The summation in Eq. (A.31) can be replaced by an integral over the phase constant surfaces (each containing $N_xN_y/2$ pq pairs). Using the notations of Eq. (38), one obtains

$$\tau(\omega) = \frac{32\pi}{Ak_1^2}\sum_n\left\langle \frac{\mathrm{Im}\{D^{(1)}_{\mathrm{rad},n}(\varepsilon_x,\varepsilon_x)\}\mathrm{Im}\{D^{(2)}_{\mathrm{rad},n}(\varepsilon_x,\varepsilon_x)\}}{|N_xN_y((1+\mathrm{i}\eta)\Omega_n^2(\varepsilon_x,\varepsilon_x)-\omega^2)+2D^{(1)}_{\mathrm{rad},n}(\varepsilon_x,\varepsilon_x)+2D^{(2)}_{\mathrm{rad},n}(\varepsilon_x,\varepsilon_x)|^2}\right\rangle_{\varepsilon_x,\varepsilon_y}, \tag{A.34}$$

where A is the area of the wetted face over a unit periodic cell. The n summation runs over the number of phase constant surfaces. The difference between this results and Eq. (38) obtained from a wave approach can be traced to the coherent grouping of the modes employed in the modal derivation.

References

[1] R.H. Lyon, R.G. DeJong, *Theory and Application of Statistical Energy Analysis*, second ed., Butterworth-Heinemann, Boston, 1995.
[2] F. Fahy, Statistical energy analysis: a critical overview, *Philosophical Transactions of the Royal Society of London A* 346 (1994) 431–447.

[3] P.W. Smith, R.H. Lyon, Sound and structural vibration, NASA Contractor Report CR-160, 1965.
[4] L. Cremer, M. Heckl, E.E. Ungar, *Structure-Borne Sound: Vibration and Sound Radiation at Audio Frequencies*, second ed., Springer, Berlin, 1988.
[5] *VA One 2007 User's Guide*, ESI Group, Paris, France, June 2007.
[6] P.J. Shorter, Wave propagation and damping in linear viscoelastic laminates, *Journal of the Acoustical Society of America* 115 (2004) 1917–1925.
[7] P. Bremner, Vibro-acoustics of ribbed structures—a compact modal formulation for SEA models, *Proceedings of the NoiseCon Conference*, Ft. Lauderdale, Florida, 1994.
[8] L. Brillouin, *Wave Propagation in Periodic Structures*, second ed., Dover, New York, 1953.
[9] D.J. Mead, A general theory of harmonic wave propagation in linear periodic systems with multiple coupling, *Journal of Sound and Vibration* 27 (1973) 235–260.
[10] D.J. Mead, Wave propagation in continuous periodic structures: research contributions from Southampton, 1964–1995, *Journal of Sound and Vibration* 190 (1996) 495–525.
[11] A.J. Keane, W.G. Price, Statistical energy analysis of periodic structures, *Proceedings of the Royal Society of London A* 423 (1989) 331–360.
[12] R.S. Langley, On the modal density and energy flow characteristics of periodic structures, *Journal of Sound and Vibration* 172 (1994) 491–511.
[13] R.S. Langley, J.R.D. Smith, F.J. Fahy, Statistical energy analysis of periodically stiffened damped plate structures, *Journal of Sound and Vibration* 208 (1997) 407–426.
[14] Y.K. Tso, C.H. Hansen, The transmission of vibration through a coupled periodic structure, *Journal of Sound and Vibration* 215 (1998) 63–79.
[15] S. Finnveden, Evaluation of modal density and group velocity by a finite element method, *Journal of Sound and Vibration* 273 (2004) 51–75.
[16] R.S. Langley, A note on the force boundary conditions for two-dimensional periodic structures with corner freedoms, *Journal of Sound and Vibration* 167 (1993) 377–381.
[17] R.R. Craig, *Structural Dynamics, an Introduction to Computer Methods*, Wiley, New York, 1981 (Chapter 19).
[18] R.S. Langley, The response of two-dimensional periodic structures to point harmonic loading, *Journal of Sound and Vibration* 197 (1996) 447–469.
[19] E.G. Williams, J.D. Maynard, Numerical evaluation of the Rayleigh integral for planar radiators using the FFT, *Journal of the Acoustical Society of America* 72 (1982) 2020–2030.
[20] F. Fahy, *Sound and Structural Vibration: Radiation, Transmission and Response*, Academic Press, San Diego, 1997.
[21] C.H. Oppenheimer, S. Dubowsky, A radiation efficiency for unbaffled plates with experimental validation, *Journal of Sound and Vibration* 199 (1997) 473–489.
[22] W.R. Graham, The influence of curvature on sound radiated by vibrating panels, *Journal of the Acoustical Society of America* 98 (1995) 1581–1595.
[23] B. Brouard, D. Lafarge, J.F. Allard, A general method of modelling sound propagation in layered media, *Journal of Sound and Vibration* 183 (1995) 129–142.
[24] W.R. Graham, A comparison of models for the wavenumber–frequency spectrum of turbulent boundary layer pressures, *Journal of Sound and Vibration* 206 (1997) 541–565.
[25] B. Arguillat, D. Ricot, G. Robert, C. Bailly, Measurements of the wavenumber–frequency spectrum of wall pressure fluctuations under turbulent flows, *Proceedings of the 11th AIAA/CEAS Aeroacoustics Conference*, Monterey, California, 2005.
[26] P.J. Shorter, R.S. Langley, On the reciprocity relationship between direct field radiation and diffuse reverberant loading, *Journal of the Acoustical Society of America* 117 (2004) 85–95.
[27] E. Nilsson, A.C. Nilsson, Prediction and measurement of some dynamic properties of sandwich structures with honeycomb and foam cores, *Journal of Sound and Vibration* 251 (2002) 409–430.
[28] L.J. Gibson, M.F. Ashby, *Cellular Solids*, second ed., Cambridge University Press, Cambridge, 1997.
[29] K. Renji, P.S. Nair, Modal density of composite honeycomb sandwich panels, *Journal of Sound and Vibration* 195 (1996) 687–699.
[30] A.C. Nilsson, Wave propagation in and sound transmission through sandwich plates, *Journal of Sound and Vibration* 138 (1990) 73–94.
[31] G. Venzke, P. Dammig, H.W. Fischer, The influence of stiffeners on the sound radiation and transmission loss of metal walls, *Acustica* 29 (1973) 29–40 (in German).
[32] F.G. Leppington, E.G. Broadbent, K.H. Heron, The acoustic radiation efficiency of rectangular panels, *Proceedings of the Royal Society of London A* 382 (1982) 245–271.
[33] R.S. Langley, The modal density and mode count of cylinder and curved panels, *Journal of Sound and Vibration* 169 (1994) 43–53.
[34] L.R. Koval, Effect of air flow, panel curvature, and internal pressurization on field-incidence transmission loss, *Journal of the Acoustical Society of America* 59 (1976) 1379–1385.
[35] B.R. Mace, P.J. Shorter, Energy flow models from finite element analysis, *Journal of Sound and Vibration* 233 (2000) 369–389.